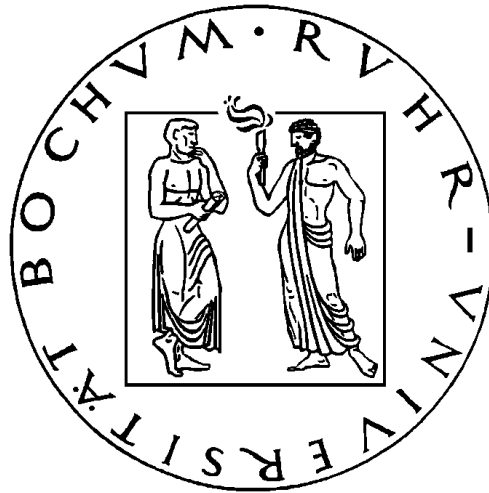


The ISO–2MASS AGN Survey



DISSERTATION

zur Erlangung des Grades
„Doktor der Naturwissenschaften“
der Fakultät für Physik und Astronomie
an der Ruhr–Universität Bochum

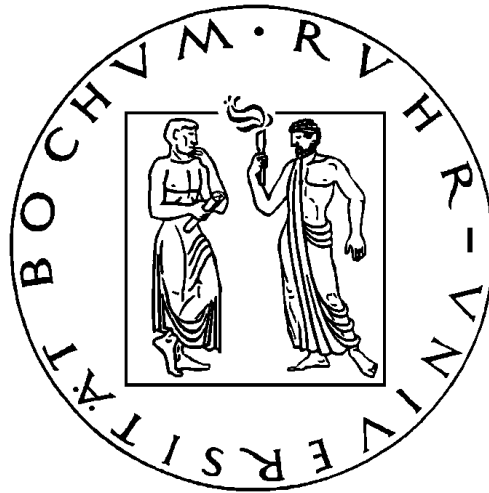
vorgelegt von
Christian Leipski

Bochum 2006

Erster Gutachter: Prof. Dr. Rolf Chini
Zweiter Gutachter: Dr. habil. Martin Haas

Disputation: 04.07.2006

The ISO–2MASS AGN Survey



PHD THESIS

Faculty of Physics and Astronomy
Ruhr–University Bochum

Christian Leipski

Bochum 2006

First referee: Prof. Dr. Rolf Chini

Second referee: Dr. habil. Martin Haas

Defense: 04.07.2006

Contents

1. Introduction	1
1.1 Background	1
1.2 The Unified Model	2
1.3 The selection of AGN	5
1.3.1 The search for obscured AGN	5
1.4 Motivation	6
1.5 Layout of the thesis	6
2. Observations and data reduction	9
2.1 Catalogue data	9
2.2 Optical spectroscopy	9
2.3 Near-infrared photometry	10
2.4 Mid-infrared spectroscopy	11
3. Mid-infrared selection of AGN	13
3.1 Selection of MIR sources	14
3.2 AGN candidate selection	15
3.3 Optical spectroscopy	19
3.4 Conclusions	20
4. The ISO-2MASS AGN survey: On the type-1 sources	23
4.1 Results and discussion	24
4.1.1 Properties of the ISO-2MASS AGN	24
4.1.2 Comparison with optical-UV selected QSOs	27
4.1.3 Comparison with the 2MASS red AGN survey	30
4.2 The nature of the ISO-2MASS type-1 QSOs	31
5. The reddest ISO-2MASS quasar	33
5.1 Results and Discussion	33
5.1.1 The quasar	34

5.1.2	The companion	38
5.1.3	Comparison with other red quasars	38
5.1.4	The nature of J2341	40
5.2	Conclusions	40
6.	Narrow-line AGN in the ISO-2MASS Survey	43
6.1	Type-2 candidates	43
6.2	Results and Discussion	44
6.2.1	J0441	44
6.2.2	J1232	45
6.2.3	Comparison of type-1 and type-2 objects	49
6.3	Conclusions	50
7.	Summary and outlook	51
7.1	Summary	51
7.2	Outlook	52
	Bibliography	53
	Curriculum Vitae	57

List of Figures

1.1	Example spectrum of a type-1 and a type-2 AGN	2
1.2	Spectropolarimetry of NGC 1068	3
1.3	The Unified Model	4
3.1	SED of the quasar 3C351	14
3.2	MIR spectrum of the star forming galaxy NGC 891	15
3.3	NIR colour-colour diagrams	16
3.4	Optical spectra of three ISOCP sources	21
4.1	IR colour-colour diagram of the ISO-2MASS AGN	24
4.2	Distribution of K_s magnitude and redshift for type-1 QSOs	25
4.3	SEDs of the six ISO-2MASS QSOs with SDSS photometry	26
4.4	Mean SEDs of different QSO samples	27
4.5	QSO number counts of the ISO-2MASS and three optical surveys	30
5.1	R-band image and spectra of J2341 and its companion	35
5.2	Comparison of J2341 with the mean SDSS quasar template	36
5.3	Blue portion of the spectra of the quasar and its companion	37
5.4	IRS/Spitzer spectrum of J2341	38
6.1	Optical and MIR spectra of two ISO-2MASS type-2 AGN	44
6.2	Enlarged view of the optical continuum of J0441 and J1232	46
6.3	Comparison of the MIR spectra of J0441, M 82, and Mrk 273	47
6.4	K_s versus z distribution for the ISO-2MASS AGN	48
6.5	[O III] luminosity versus absolute K_s magnitude	49

List of Tables

3.1	Mean NIR colours of comparison samples	17
4.1	Parameters of the ISO–2MASS type–1 QSOs	29
4.2	Number counts of the IR and optical QSO samples	32
5.1	Line fluxes and luminosities of narrow emission lines in J2341	34
5.2	Photometry of the J2341 system	39
6.1	Parameters of the ISO–2MASS type–2 AGN	45

Abstract

This thesis presents a new approach to select active galactic nuclei (AGN) using the unique MIR data provided by the *ISOCAM Parallel Mode Survey*.

While optical and UV–excess surveys for AGN are biased against dust reddened objects, investigations at radio and X–ray wavelengths have demonstrated that a significant number of obscured AGN in fact exist. The reemission of the hiding dust, however, can be detected at infrared wavelengths. Therefore, the *ISOCAM Parallel Mode Survey* at $6.7\ \mu\text{m}$ (*LW2* filter) is combined with the *Two Micron All Sky Survey* (2MASS) in order to obtain a powerful tool to search for AGN independent of dust extinction. The results are:

- Using suitable comparison samples moderate colour criteria were determined and used to select a sample of 77 AGN candidates in an effective area of ~ 10 square degrees.
- By means of optical follow–up spectroscopy different types of AGN, including obscured sources, were identified. It turns out that about one third of the ISO–2MASS AGN show so red optical colours that they are missed in classical surveys. These additional red objects cause the surface density of the ISO–2MASS AGN to outnumber that of the (optical) SDSS survey by 50%.
- The detailed study of the reddest ISO–2MASS quasar reveals an interacting system. The analysis of optical and MIR spectra demonstrates that the quasar lacks the AGN continuum in the optical while the emission lines are essentially unabsorbed. A possible explanation is the presence of a compact absorber near the continuum source.
- Studying the narrow–line AGN found by the ISO–2MASS survey the diversity of type–2 spectra at optical as well as at MIR wavelengths is emphasised. Comparing the type–1 with the type–2 sources it is shown that type–2s are underrepresented by a factor of three in our survey. However, at $z < 0.5$ the numbers for different AGN types are similar. It is discussed that this might be due to orientation and obscuration effects that result in high– z type–2s missing the ISO–2MASS magnitude limit.

To conclude, the optically inferred number density of AGN has to be revised due to a significant population of reddened AGN. The high diversity in the spectra of narrow–line AGN implies that these sources are hard to find systematically at optical wavelengths. Finally, the ISO–2MASS AGN survey proves to invent an effective method to select AGN regardless of their type and level of obscuration.

Introduction

1.1 Background

Active Galactic Nuclei (AGN) produce large amounts of energy on scales probably smaller than 1 pc^3 . The luminosity is emitted over a broad range of wavelengths (from radio to X-rays) and can easily exceed the luminosity of a typical galaxy. Depending on the luminosity AGN are referred to as quasars and their less powerful siblings are called Seyfert galaxies¹.

AGN are powered by a luminous central engine, most likely an accreting supermassive black hole (BH). Driven by gravitational pull, matter spirals towards the black hole and its potential energy is converted into thermal radiation in an accretion disk. There the UV/optical radiation that can be observed directly as prominent blue continuum emission is produced. The strong radiation field of the AGN also heats circum nuclear dust that subsequently re-radiates the absorbed energy as continuum emission in the infrared (IR). Strong X-ray emission from a hot corona above the accretion disc as well as emission of a radio jet emerging from the centre may also be observed in AGN.

The defining characteristics of AGN, as used in essentially all optical surveys to identify them, are their (optical) broad and narrow emission lines. These are presumably produced by the central continuum source through photoionisation of gas near the BH. The gas is thought to be condensed in individual clouds performing orbital motions around the centre. The kinematical broadening of the observed emission lines therefore depends on the distance from the black hole leading to the identification of the broad-line region (BLR) and the narrow-line region (NLR). The BLR is represented by broad emission-lines (several 1000 km/s FWHM) from gas located near the centre. The NLR is characterised by narrow emission lines (few 100 km/s FWHM) from gas further out

¹ The distinction between quasars and Seyferts is made at $M_B = -23 \text{ mag}$. Strictly speaking AGN brighter than this limit are called quasi-stellar objects (QSOs) while the radio-loud part of this population is called quasi-stellar radio source (quasar). However, these terms are used almost synonymously in the literature for describing radio-quiet as well as radio-loud object and both terms will be used to refer to an AGN of high luminosity, regardless of its radio loudness.

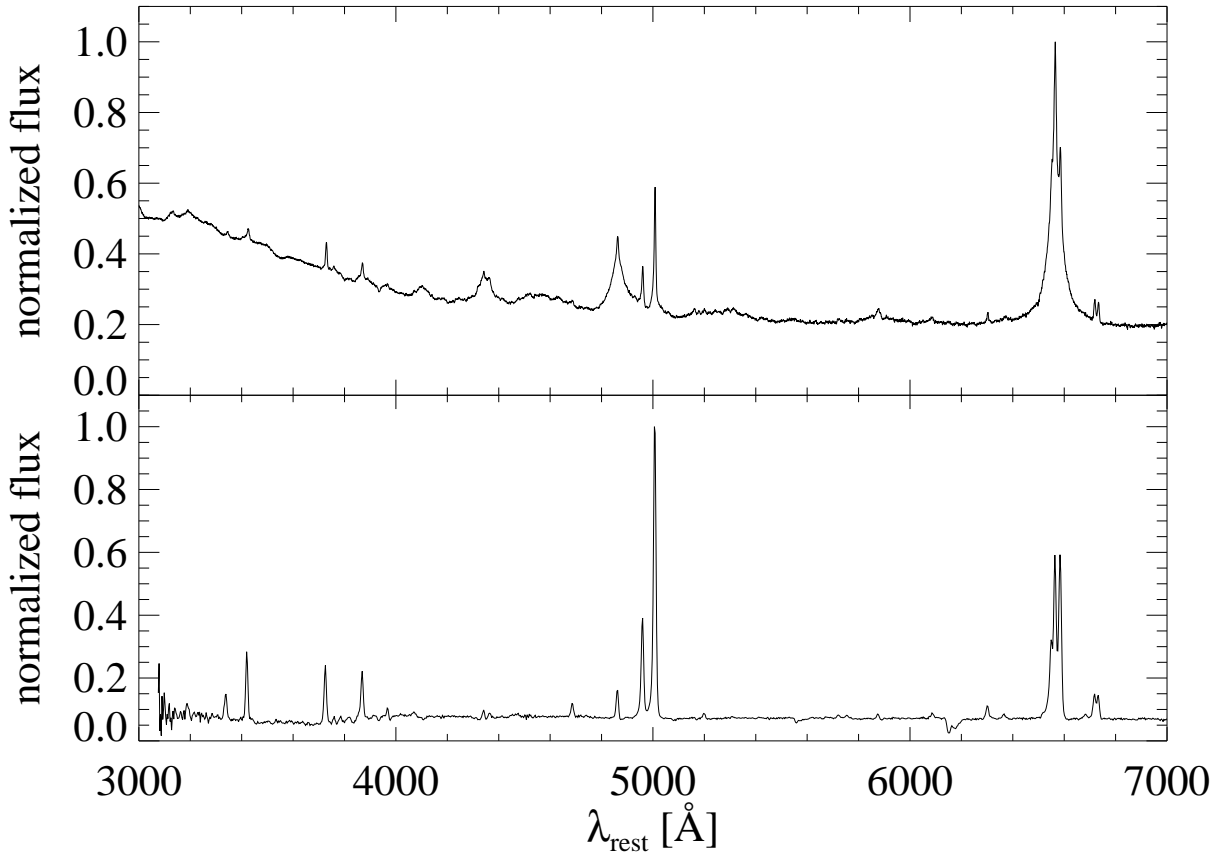


Figure 1.1: *Top*: Example spectra for a type-1 AGN. The broad Balmer and narrow forbidden lines are clearly visible, as well as the blue optical continuum (Vanden Berk et al. 2001). *Bottom*: Example spectrum of a type-2 AGN. All the emission lines are narrow and almost of the same FWHM. Type-2 AGN lack the rising optical continuum seen in type-1 objects.

in the galaxy. Thereby only permitted lines are observed of broad as well as of narrow line width. Forbidden lines on the other hand are always narrow. Because of the high electron density in the BLR forbidden transitions are collisionally deexcited before they can emit radiation.

1.2 The Unified Model

Broadly speaking, the AGN population can be divided by the presence or absence of broad emission lines². While type-1 AGN show broad and narrow emission lines in their spectra, type-2 AGN only show narrow emission lines (Fig. 1.1). Additionally, type-1 AGN often show a strong blue optical continuum in contrast to type-2 AGN, where

² This classification scheme may be further subdivided according to the Balmer emission-line profiles (e.g. Osterbrock 1977).

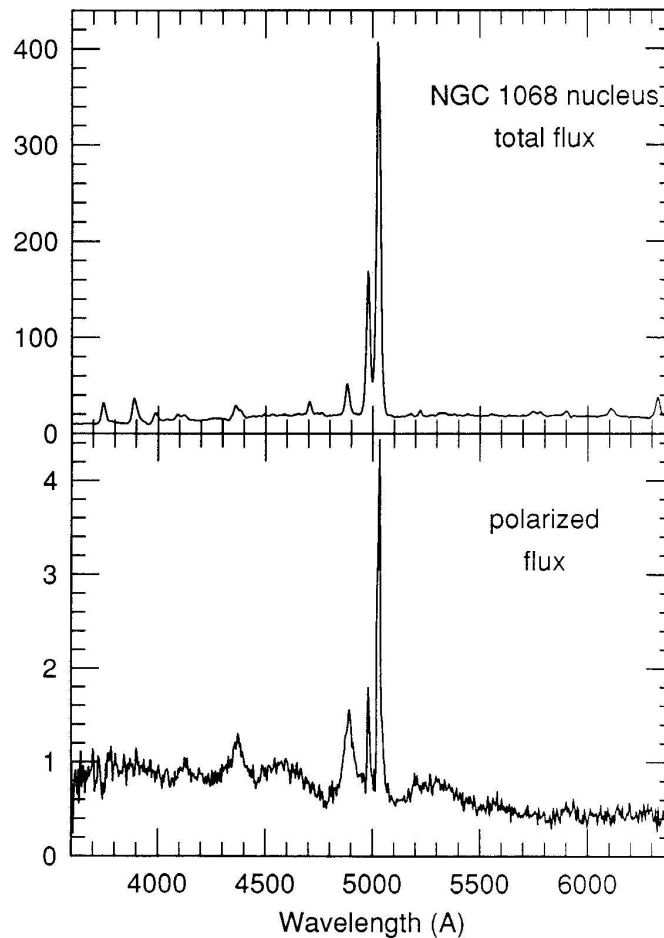


Figure 1.2: Spectropolarimetry of NGC 1068 taken from Miller et al. (1991). The broad emission lines present in the polarised flux are clearly visible. Light from the BLR is scattered into the line of sight enabling a periscopic view into the central regions that are hidden in direct light.

this continuum is usually weak or absent and difficult to disentangle from the stellar continuum of the host galaxy.

The observation of broad emission lines in the polarised flux of NGC 1068 (Antonucci & Miller 1985) led to the realization that orientation affects the classification of AGN (Fig. 1.2). In the framework of the so called Unified Model (Antonucci 1993) type-1 and type-2 AGN are intrinsically the same objects but viewed under different angles. Around the source of the (UV/optical) continuum emission there is supposed to exist a dusty torus (Fig. 1.3). Viewed edge-on the torus hides the continuum source and the BLR. In this case only the narrow emission lines from the more extended NLR are observed and the object is classified as a type-2 AGN. A face-on view allows the continuum source as well as the BLR to be observed. Now a type-1 AGN is observed with a blue continuum as well as broad emission lines in addition to the NLR emission lines (Fig. 1.1).

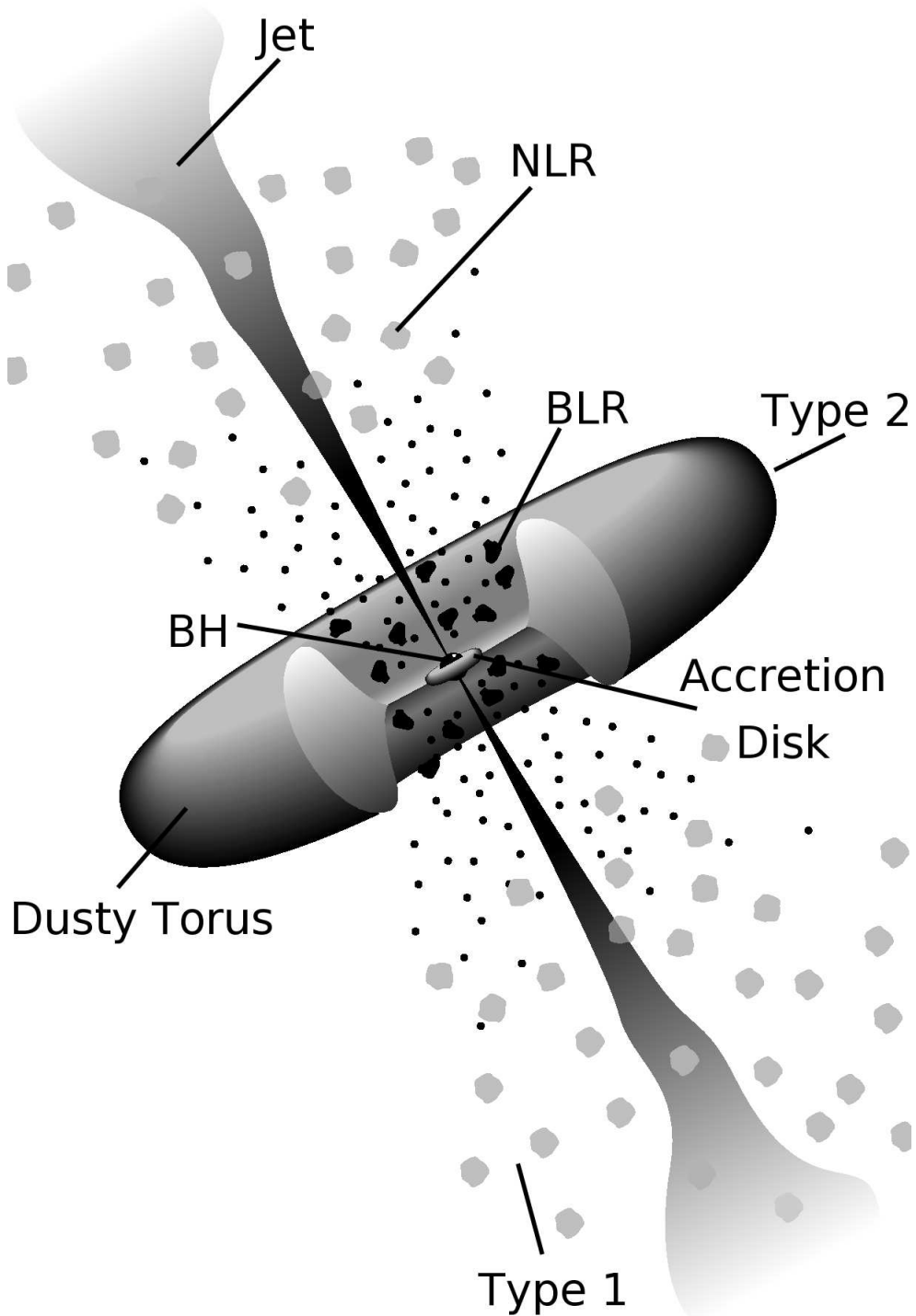


Figure 1.3: Schematic illustration of the unified model for AGN (Urry & Padovani 1995).

1.3 The selection of AGN

Most techniques used to search for AGN rely on the fact that the optical spectra of AGN differ in shape from those of stars and normal galaxies, especially at high luminosities. The prominent UV/optical AGN continua (Fig. 1.1) allow the selection of AGN based on their colours in broad-band photometric filters. One of the best known samples using such a technique is the Palomar Bright Quasar Survey of Schmidt & Green (1983). These authors were searching for pointlike objects exhibiting an “UV-excess”, i.e. having blue $U - B$ colours. Although over 100 AGN have been identified in this shallow survey, the technique suffers from considerable contamination by hot subdwarfs (40%) and white dwarfs (20%).

With the advent of deep large area surveys like the Sloan Digital Sky Survey (SDSS, York et al. 2000) the selection techniques have been advanced using multi-colour criteria. Considering the shape of the continuum as well as the emission lines, the colours of AGN are determined with respect to their redshift. In colour-colour diagrams of the five SDSS filters (*ugriz*) appropriate candidates are selected to lie outside the stellar loci, i.e. the region in colour space where most stars reside (Richards et al. 2002). The major problems of such a selection technique is that they rely on a template spectrum to derive the colours according to the redshift. Sources that differ from that template are not selected. Especially it is expected that dust-reddened quasars lack significant amounts of the AGN continuum and their colours resemble those of stars, i.e. they can not be distinguished from other objects inside the stellar locus by optical techniques alone.

1.3.1 The search for obscured AGN

To identify the entire AGN population independent of dust extinction, surveys in the radio, in X-rays and in the infrared have been carried out. However, only about 30% of the AGN are radio-loud (Urry & Padovani 1995) and there seem to exist many X-ray faint AGN (Wilkes et al. 2002).

On the other hand the reemission of the hiding dust which is heated by the strong radiation field of the AGN, should be seen in the mid-IR as continuum emission (e.g. Meisenheimer et al. 2001; Haas et al. 2003).

Already at far-infrared (FIR) wavelengths searches for warm FIR colours typical for AGN have indicated that optical surveys may miss a significant fraction of the AGN population (Low et al. 1988).

One of the best known samples of infrared selected AGN are the 2MASS red AGN (Cutri et al. 2001). These sources have $J - K > 2$, i.e. a very red NIR continuum that can either be explained by emission from very hot dust or by strong reddening of the NIR continuum. However, the design of the survey was to look for extreme sources that are missed in optical surveys. Subsequently it has been shown that the colour selection via $J-K > 2$ excludes most of the known AGN (Barkhouse & Hall 2001).

Also in the MIR ($\approx 5 - 40 \mu\text{m}$) searches for AGN have been started. At these wavelengths AGN in general are dominated by continuum emission from hot dust heated

by the intense radiation field. The major task in the MIR however is to disentangle AGN from starburst galaxies that also have considerable MIR and FIR emission, but usually with cooler colours and different spectral shapes (Laurent et al. 2000; Lacy et al. 2004a).

The advantage of search techniques using isotropic properties as in the MIR is that classical type-1 sources as well as reddened type-1s and type-2 sources (i.e. heavily obscured type-1s according to the unified model) can be found.

In the optical, obscured type-1 and type-2 AGN are hard to select, because they lack the defining AGN continuum. However, the (optically thin) emission of dust heated by the hidden continuum source can be detected at infrared wavelengths, enabling searches for type-1 as well as for type-2 AGN.

In general, the results of searches at various wavelengths demonstrates that a considerable fraction of the AGN population is missed due to observational bias.

1.4 Motivation

The availability of the *ISOCAM Parallel Mode Survey* (e.g. Cesarsky et al. 1996; Siebenmorgen et al. 1996; Ott et al. 2003, 2006) gives us the possibility to benefit from a large data set of $6.7\ \mu\text{m}$ data on high galactic latitude objects. The combination with the 2MASS point source catalogue (Cutri et al. 2003) makes a unique tool to search for hitherto unknown populations of AGN. An unusually high $6.7\ \mu\text{m}$ MIR excess over the NIR fluxes of 2MASS directly suggests a connection with the sought-after hidden AGN population. Therefore a new approach to search for AGN by means of their near- and mid-IR emission properties of the nuclear dust torus is proposed.

1.5 Layout of the thesis

The main results cover different aspects that are presented in chapters 3 to 6. These chapters individually provide new insights on AGN in general and on AGN selection in particular. Therefore the findings have been and will be published chapterwise.

Except AGN also dusty star forming galaxies may show strong near- and mid-infrared emission and some contamination of the sample by these sources is expected. But in this thesis I will focus on the AGN and the results on star forming galaxies will be addressed briefly in the outlook. The thesis is organized as follows:

Chapter 2 presents the data that have been obtained to study the selected AGN candidates.

Chapter 3 introduces the technique to select AGN at NIR/MIR wavelengths. The initial data set is presented as well as the detailed procedure to exclude contamination by other astronomical objects like stars, normal galaxies, and ultra-luminous infrared galaxies (ULIRGs). First results from optical follow-up spectroscopy confirm the approach.

In **Chapter 4** first findings of the survey are discussed. The results of the complete optical follow-up spectroscopy of the ISO-2MASS AGN candidates are presented. Fo-

using on the type-1 sources their properties and number densities are compared with those of optical surveys.

In **Chapter 5** the reddest type-1 quasar unveiled by the ISO-2MASS AGN survey is explored in detail. The optical and MIR spectra are studied as well as results from optical and NIR imaging. The special geometry that is necessary to explain the observational results in the framework of the unified model is discussed. Alternative explanations are presented as well as a comparison with the NIR selected red 2MASS AGN.

In **Chapter 6** the type-2 AGN are studied by means of optical and MIR spectroscopy. Two representative sources are used to demonstrate the diversity in the spectra and to study the different stellar populations and the state of star formation.

In **Chapter 7** the results are summarised and a brief outlook is given.

Chapter 2

Observations and data reduction

2.1 Catalogue data

Mid-infrared photometry of $\sim 17\,000$ sources was provided by the *ISOCAM Parallel Mode Survey* (Cesarsky et al. 1996; Siebenmorgen et al. 1996; Ott et al. 2006). This serendipitous survey was performed with *ISCOAM* at $6.7\ \mu\text{m}$ (*LW2* filter) in its parallel mode while another instrument was prime.

The combination with the *Two Micron All Sky Survey* (2MASS, Cutri et al. 2003) yield JHK_s photometry for all MIR sources with NIR counterparts down to a magnitude limit of $K_s < 15.5$ mag.

Optical photometry in the filters B and R was provided by *USNO-B1.0* (Monet et al. 2003). Only sources with a MIR, NIR, *and* optical counterpart were selected for the candidate selection process.

The NIR and optical catalogues also provided coordinates of the sources with estimated accuracies of $\sim 0''.2$ at J2000 (e.g. Monet et al. 2003).

For a subset of the survey sources photometric data from the *Sloan Digital Sky Survey* (SDSS, York et al. 2000) data releases 3 and 4 (Abazajian et al. 2003; Adelman-McCarthy et al. 2006) were available.

2.2 Optical spectroscopy

To establish the nature and the redshift of the 77 AGN candidates selected in the course of this thesis, low-resolution optical spectroscopy of 69 of them was performed. For the eight remaining sources these information were already available.

Additionally optical spectra of suitable comparison samples to test our selection technique were obtained. These samples were from neighbouring regions in the NMIR colour-colour diagram as used to select the AGN candidates. These regions are supposed to be populated by certain kinds of astronomical objects and, thus, can serve as a test for the colour criteria.

The optical spectroscopy has been obtained with the given instrument at the following observatories/telescopes:

- European Southern Observatory (ESO) NTT/EMMI
- ESO VLT/FORS1
- Calar Alto 2.2 m with CAFOS
- Kitt Peak National Observatory (KPNO) 2.1 m with GoldCam
- Cerro Tololo Inter-American Observatory (CTIO) 4 m-Blanco with the R-C Spectrograph
- Nordic Optical Telescope (NOT) with ALFOSC
- Telescopio Nazionale Galilei (TNG) with DOLORES
- South African Astronomical Observatory (SAAO) 1.9 m with the Grating Spectrograph
- Thüinger Landessternwarte Tautenburg (TLS) 2 m with the faint-object Nasmyth Spectrograph

The spectroscopic data reduction was performed in the standard manner using ESO/MIDAS version 04FEBpl1.0.

The redshifts of the sources were derived from the position of observed emission lines. If several emission lines were present the redshift values were checked for consistency.

Objects with broad emission lines ($\text{FWHM} \geq 2500 \text{ km s}^{-1}$) were identified as the type-1 AGN population. For the narrow-line objects the emission-line fluxes were determined using gaussian fits to the emission-line profiles. Emission-line ratio diagrams distinguish between (narrow-line) type-2 AGN and emission-line galaxies (Veilleux & Osterbrock 1987; Kewley et al. 2001).

2.3 Near-infrared photometry

For the detailed study of the reddest quasar in the survey near-infrared imaging photometry was obtained using ISPI at the CTIO 4 m-Blanco telescope. The data were reduced with IRAF using standard techniques. Photometric calibration was performed with stars in the field that are measured by 2MASS. By means of aperture photometry the JHK_s magnitudes of the object were determined. Since the quasar turned out to be a double source (chapter 5), photometry of the quasar alone was obtained after subtracting the faint companion using a point-spread function (PSF) build from stars in the field.

2.4 Mid-infrared spectroscopy

For a representative subset of the sample also low-resolution MIR spectra from 5–38 μm have been obtained (program id 3231) using IRS (Houck et al. 2004) aboard *Spitzer Space Telescope* (Werner et al. 2004). The Basic Calibrated Data (BCD-files) were background corrected manually by pairways subtraction of two nod positions along the slit. The data were then extracted and calibrated using *SPICE*¹.

By this procedure, one gets four spectra for each nod position and each cycle covering the whole wavelength range of IRS². These spectra have been flagged (i.e. residuals and spikes have been removed), combined, and averaged to a single spectrum covering the full spectral range.

¹ The “Spitzer IRS Custom Extraction” (*SPICE*) is JAVA-based tool that allows the user to interactively extract IRS spectra. The software is provided by the *Spitzer Science Center*.

² The short-low (SL) resolution mode of IRS provides low-resolution spectroscopy from 5.2 to 14.5 μm covered by two orders. The long-low (LL) mode provides the 14.0 to 38.0 μm range also by two orders.

Mid-infrared selection of AGN

The realisation that obscuration plays a critical role in the classification of AGN fundamentally inspired the current research. Attempts to overcome the limitations of dust extinction and to identify the entire AGN population – including type-2 and dust-enshrouded AGN – encompass surveys in the near-IR, radio, and X-ray regimes. However, searching for very red AGN the colour selection via $J - K_s > 2$ Cutri et al. (2001) excludes most of the known AGN (Barkhouse & Hall 2001), only about 30% of AGN are radio-loud (Urry & Padovani 1995), and there seems to exist many X-ray faint AGN (Wilkes et al. 2002). Thus, a considerable fraction of the AGN population must have escaped detection due to observational bias.

Webster et al. (1995) found that their radio-selected quasar sample is significantly redder than an optical comparison sample and concluded that up to 80% of the quasars have been missed in conventional optical surveys, provided that the redder colours of the radio-loud quasars are due to dust reddening and that the radio-quiet quasars contain as much dust as the radio-loud ones.

By new strategies in the optical, assuming that the narrow-line regions are sufficiently extended and that only the continuum emission is hidden, type-2 quasar candidates have been selected as objects with narrow permitted emission lines and high $[\text{O III}]\lambda 5007$ equivalent widths (Djorgovski et al. 2001; Zakamska et al. 2003). Applying a moderate colour cut $J - K_s > 1.2$, from about 1500 sources in 2MASS Francis et al. (2004) find only tentative evidence that Seyfert 2 nuclei are more common in the NIR selected survey than in blue selected galaxy surveys, and they can place only very weak constraints on any population of dusty AGN.

The disadvantage of heavy extinction in optical and NIR surveys can turn into a valuable detection tool, when observing dust-surrounded AGN at MIR wavelengths. There, the reemission of the hiding dust heated by the strong radiation field of the AGN should be seen easily as MIR excess. In fact, for known (powerful) AGN of both type-1 and type-2 a steep near- to mid-IR slope has been revealed by sensitive MIR

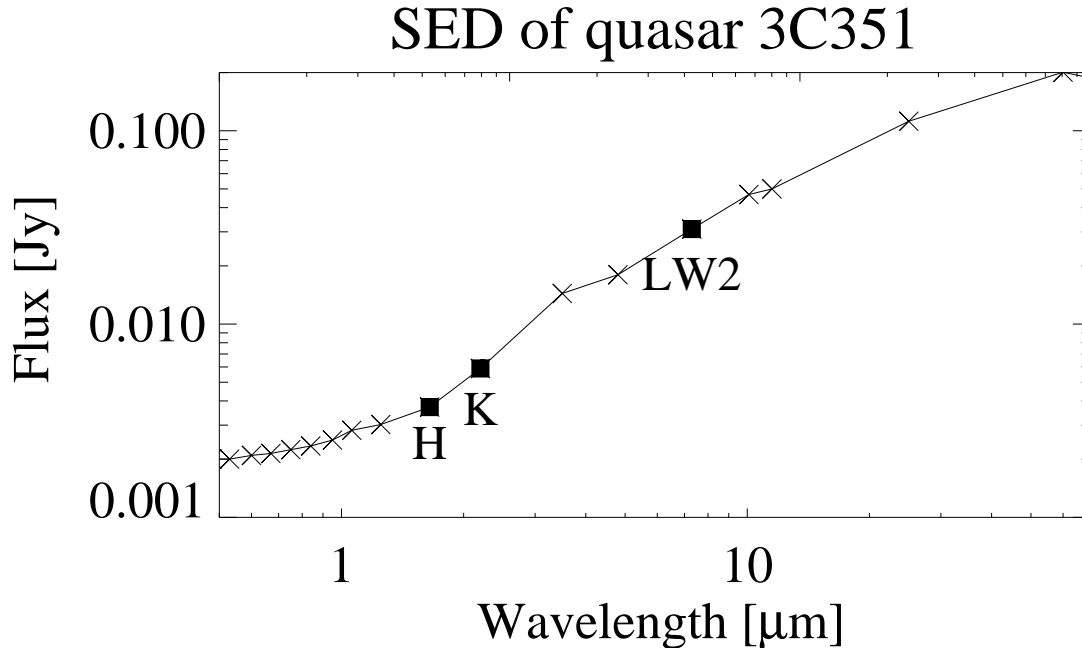


Figure 3.1: SED of the quasar 3C351. The rising continuum due to hot dust emission powered by the AGN is clearly visible.

observations (Fig. 3.1; e.g. Haas et al. (2003, 2004b); Siebenmorgen et al. (2004)).

We therefore started a new approach, searching for AGN by means of their MIR emission of the nuclear dust torus. However, one complication with this method has to be solved: Since luminous IR starburst galaxies may also show a pronounced MIR emission due to the PAH emission bands around $7.7 \mu\text{m}$ (Fig. 3.2), it is of special importance to distinguish them from AGN. In this chapter we describe the new technique for the mid-IR selection of AGN candidates using IR colour diagrams and report about first results from optical spectroscopy.

3.1 Selection of MIR sources

ISO has performed a serendipitous survey at $6.7 \mu\text{m}$ (*LW2* band), the *ISOCAM Parallel Survey*, with $6''$ spatial resolution and a positional accuracy of better than $3''$ (Siebenmorgen et al. 1996; Ott et al. 2003). Over 27 square degrees of the sky are processed and currently being catalogued. For point sources the 3σ detection limit is about 0.5 mJy.

Within the scientific verification of the 17000 detected sources (Ott et al. 2006) we have selected unresolved sources at galactic latitude $|b| > 20^\circ$. We then performed cross correlations with the 2MASS all sky point source catalogue (Cutri et al. 2003), with the USNO-B, DSS and UCAC optical catalogues, as well as the NVSS and FIRST radio surveys, and analysed IRAS ADDSCANS. We excluded objects which have multiple NIR and optical counterparts within $10''$, or are contaminated by extended sources

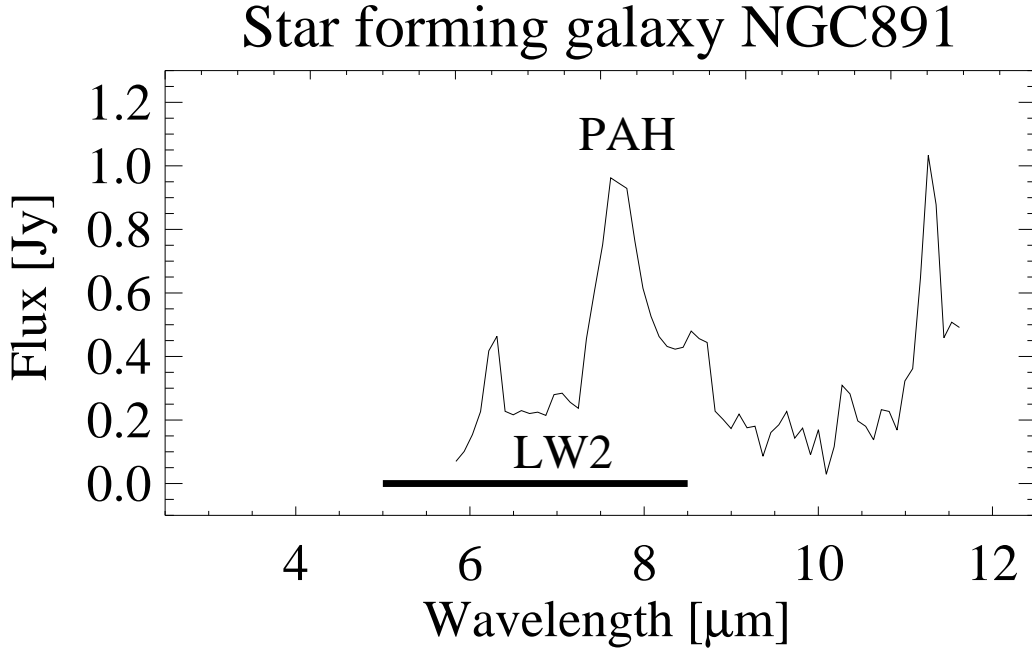


Figure 3.2: MIR spectrum of the star forming galaxy NGC 891. The width of the *LW2* filter is also indicated. Most of the features visible in this spectrum are from PAHs and it is obvious that the amount of PAH emission strongly influences the *LW2* magnitude.

(2MASS XSC), or have proper motion ($pm > 3\sigma$ from UCAC). The resulting list contains about 3000 ISOCAM point sources with *BRJHK* and *LW2* ($6.7\ \mu\text{m}$) photometry (henceforth denoted ISOCP sources). The brightness ranges are: $B = 14.5 \dots 20.5$ mag, $K_s = 12.5 \dots 16$ mag, $LW2 = 8 \dots 12$ mag $\pm 0.2 \dots 0.4$ (Vega based system). The typical errors on the $H - K_s$ and $K_s - LW2$ colours are $0.1 \dots 0.2$ mag and $0.3 \dots 0.5$ mag, respectively.

3.2 AGN candidate selection

The ISOCP list contains various object classes like stars, normal and active galaxies. Fig. 3.3 (top) shows their distribution in the $H - K_s$ versus $K_s - LW2$ colour-colour diagram. Noteworthy, the ISOCP sources clearly reach more extreme IR colours than those of the Hubble Deep Field South (Oliver et al. 2002; Mann et al. 2002) and the ELAIS fields (Väisänen et al. 2002; Rowan–Robinson et al. 2003). The corresponding limits are indicated in Fig. 3.3.

To identify the types of objects that populate different regions of the colour-colour diagram shown in Fig. 3.3 (top), we show the same diagram for sources with known identification in Fig. 3.3 (bottom). Stars, i.e. proper motion objects, lie in the lower left corner at $K_s - LW2 < 1$ and $H - K_s < 0.5$. This area also contains radio-quiet elliptical galaxies from the revised Shapley–Ames catalog.

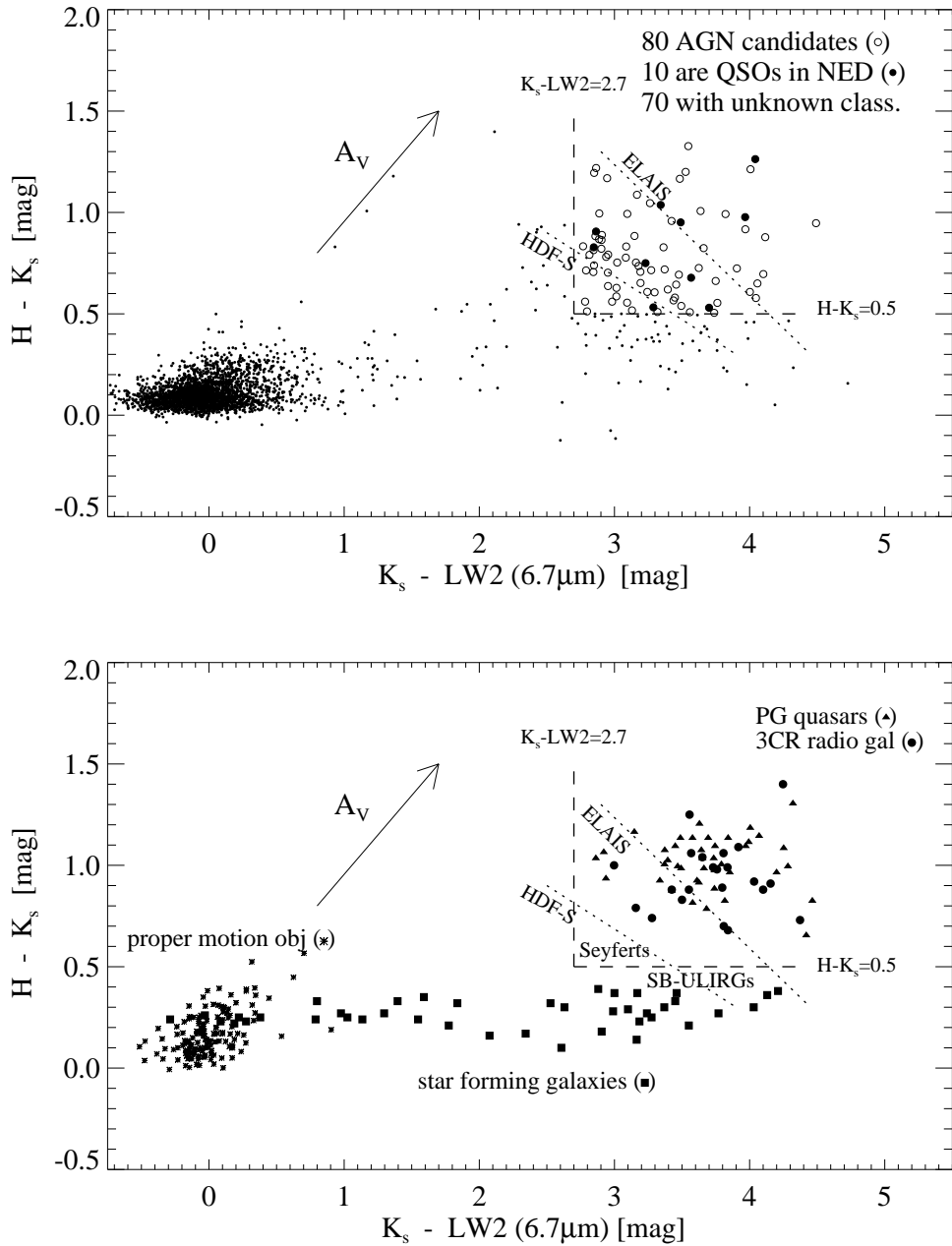


Figure 3.3: *Top:* $H - K_s$ vs. $K_s - LW2$ colour-colour diagram of the 3000 unresolved ISOCAM sources at $|b| > 20^\circ$. Circles and fat dots denote the AGN candidates, small dots all other sources. The dotted oblique lines indicate the limits reached by the HDF-S and ELAIS sources, lying below and left hand of the lines. *Bottom:* Comparison samples.

	$H - K_s$	N	$K_s - LW2$	N
Sy1 (<1.8)	0.59 ± 0.18	25	2.8 ± 0.6	25
Sy2 (≥ 1.8)	0.39 ± 0.18	23	2.7 ± 0.8	23
SBs-ULIRGs	0.49 ± 0.17	21	3.9 ± 0.5	7
AGN-ULIRGs	0.94 ± 0.35	5	3.9 ± 0.4	5

Table 3.1: Mean colours of Seyfert galaxies from Clavel et al. (2001) and ULIRGs from Klaas et al. (2001). N gives the number of objects used for deriving the two colours, respectively.

UV-excess selected Palomar-Green (PG) quasars (AGN type-1, data from Haas et al. (2003)) and powerful FR 2 radio galaxies from the 3CR catalogue (AGN type-2, data from Haas et al. (2004b) and Siebenmorgen et al. (2004)) lie in the upper right corner at $K_s - LW2 > 2.7$ and $H - K_s > 0.5$ – a region that is also populated by 3CR quasars (AGN type-1). As an additional check, we cross-correlated the UV-selected quasars in the Véron-Cetty & Véron catalog (Véron-Cetty & Véron 2003, 11th edition) with the 2MASS catalog. More than 90% of the quasars with $V < 18$ mag and $z < 0.8$ lie at $H - K_s > 0.5$. At $z \sim 1.5$ the fraction goes down to 10%, probably due to the shift of the NIR excess beyond the K_s -band. The sources from the PG and the 3CR catalogs, respectively, shown in Fig. 3.3 bottom are at $z < 0.8$. For simplicity, we denote the sources in the colour range $K_s - LW2 > 2.7$ and $H - K_s > 0.5$ as excess sources.

The ISOCP excess sources are neither carbon stars (e.g. Liebert et al. 2000) nor AGB stars (Joris Blommaert, priv. comm.), both types showing optical and NIR colours different from these ISOCP sources. Also, dusty young stars show different optical colours and they are not expected at high galactic latitude $|b| > 20^\circ$.

Normal star forming galaxies (Boselli et al. 1998; Dale et al. 2001) populate the full range of $K_s - LW2$, reaching into the regime of AGN, but they lie significantly lower in $H - K_s$ (< 0.5), so that they can be distinguished from the PG/3CR AGN. Even IR luminous starburst galaxies having $10^{11} < L_{\text{FIR}} [L_\odot] < 10^{12}$, like Arp 157, NGC 1569, NGC 2146, NGC 3256 or M 82, fall into this colour range ($H - K_s < 0.5$).

Seyfert 1 and 2 galaxies, from the sample by Clavel et al. (2001) with averages listed in Tab. 3.1, lie in the “transition range” between normal star forming galaxies and PG/3CR AGN. While Sy 2s on average are below $H - K_s = 0.5$, Sy 1s are above and for clarity of the plot only the word “Seyferts” delineates their colour location in Fig. 3.3 bottom.

The colours of IR ultra-luminous ($L_{\text{FIR}} > 10^{12} L_\odot$) starburst galaxies (including LINERs), which we derived from the sample of Klaas et al. (2001) together with 2MASS and ISOCAM $6.7\mu\text{m}$ data, lie in the range $K_s - LW2 > 2.7$ and $0.2 < H - K_s < 0.8$ (Tab. 3.1). 13 of them lie below and 8 above $H - K_s = 0.5$ overlapping with the range of the PG/3CR AGN. In Fig. 3.3 only the word “SB-ULIRGs” is placed at their mean location. On the other hand, the AGN-ULIRGs with “warm” F_{12}/F_{25} colours (like Mrk 231 and IRAS 05189-2524) clearly fall into the colour range of the PG/3CR AGN (Tab. 3.1).

In following we discuss, whether the ISOCP excess sources could be explained in terms of pure starburst IR galaxies. We will argue that such star-forming galaxies would be either too bright or too distant to match *both* the observed fluxes at K_s , $LW2$ and at $60\mu\text{m}$ *and* the corresponding colours of the ISOCP excess sources. Our argumentation is essentially based upon the following empirical facts:

1. The ISOCP excess sources have median (mean) fluxes at K_s and $LW2$ of 0.66 mJy (0.9 mJy) and 1.75 mJy (3.2 mJy), respectively.
2. The $LW2$ flux of a starburst galaxy with $z < 0.15$ is mostly due to the PAH bands around $7.7\mu\text{m}$ (e.g. Laurent et al. 2000). For $z > 0.15$ this feature is shifted out of the $LW2$ passband ($5 - 8.5\mu\text{m}$) resulting in a reduced $K_s - LW2$ colour below 2.7.
3. If a red ($H - K_s > 0.5$) starburst galaxy has a $K_s -$ band excess – originating from hot dust close to the sublimation temperature – then its $60\mu\text{m}$ emission is also expected to be strong. E.g. the five SB-ULIRGs observed by Klaas et al. (2001) with $H - K_s > 0.4$ show a flux ratio $F_{60}/F_{LW2} \approx 230 \dots 570$. Less luminous, more gently star-forming galaxies might have a smaller F_{60}/F_{LW2} ratio, but – on the other hand – the typical known SB-LIRGs like M 82 are bluer ($H - K_s < 0.5$) than the present ISOCP excess sources.

PAH bands: First, we make use of the PAH bands and discuss the ISOCP excess sources with $F_{2.2\mu\text{m}} \lesssim 1$ mJy. In order to match this limit, a typical SB-ULIRG, like e.g. IRAS 17208-0014, with $F_{2.2\mu\text{m}} \approx 20$ mJy at $z = 0.042$, would have to lie at $z = 0.188$. In this case, however, $K_s - LW2$ would attain values below 2.7, see point (2.) above. The same argument applies to other SB-ULIRGs (like MRK 273, ARP 220, IRAS 14348-1447 and IRAS 23365+3604). Hence, a pure starburst counterpart of the *faint* ISOCP excess sources must have a lower luminosity, i.e. being at most an SB-LIRG.

F_{60}/F_{LW2} ratio: Second, we make use of the F_{60}/F_{LW2} ratio, which attains typically values above 230 for SB-ULIRGs. A similar flux ratio is expected for highly dust-enshrouded SB-LIRGs with $H - K_s > 0.5$ (down-sized SB-ULIRGs), if they exist. In order to match $F_{LW2} > 1$ mJy for the *bright* ISOCP sources, the expected flux at $60\mu\text{m}$ would have to be at least $F_{60} \gtrsim 230 \dots 570$ mJy, which is above the IRAS detection threshold at low-cirrus high-galactic latitudes.

For *faint* ISOCP sources with fluxes $F_{LW2} < 1$ mJy we expect useful IRAS upper limits. We have examined the 70 unclassified ISOCP excess sources (Fig. 3.3, top) individually: only eight of them show a marginal detection in the $60\mu\text{m}$ IRAS ADDSCAN data, the remaining sources have 3σ upper limits between 90 and 190 mJy. Two of the detected sources exhibit $F_{60}/F_{LW2} < 230$, all of the remaining sources have $F_{60}/F_{LW2} < 180$ and at least 40 of them even have $F_{60}/F_{LW2} < 100$. These low limits show that most of the 70 ISOCP sources are characterised by a high MIR/NIR flux ratio, which is not

accompanied by a high FIR/MIR ratio as expected for known dust–enshrouded pure starburst galaxies with $H - K_s > 0.5$.

If the ISOCP excess sources are not a new population of star–forming galaxies, which are highly dust–enshrouded (with red $H - K_s$), rich in PAH emission (with bright F_{LW2}) and have cool FIR colours (with low $60\mu\text{m}$ flux), then the arguments above favour a significant AGN contribution in these sources. Furthermore, the four AGN–ULIRGs show an F_{60}/F_{LW2} ratio between 10 and 50, consistent with the $60\mu\text{m}$ upper limits found for the ISOCP excess sources.

Based on the comparison with known object types we predict that most of the 80 ISOCP excess sources house an AGN and have Seyfert luminosities, but could be more powerful if at $z \gtrsim 0.2$. Therefore, we consider the ISOCP excess sources as promising AGN candidates. At redshift about $z > 0.8$, when the AGN–typical SED bump shifts, the colours of the sources may become bluer than $H - K_s = 0.5$, and a refined analysis using other filters has to be applied in order to identify all AGN. Remarkably, the new method is – á priori – not biased against optical–UV selected QSOs. For comparison, the 2MASS AGN search catches only the range $H - K_s > 0.7$ (roughly corresponding to the $J - K_s > 1.2$ criterion used by Francis et al. (2004), hence may ignore more of the known AGN – even among the local ones.

3.3 Optical spectroscopy

Obviously, our predictions about the nature of the ISOCP excess sources have to be verified by optical spectroscopy. Ten of our 80 AGN candidates are already listed in the NED as QSOs. None is listed as a star (in SIMBAD) or starburst galaxy. Twelve sources have 1.4 GHz radio detections, 4 being radio loud. Only one source (3C345, Sandage & Wyndham 1965) has also been identified spectroscopically as QSO in the Sloan Survey (SDSS DR1 Abazajian et al. 2003) while SDSS DR2 contains only one more spectrum of an ISOCP excess source (RA,Dec_{J2000} = 13:25:07.8, +05:41:07) – it is a QSO at $z = 0.2$.

Because of the marginal spectroscopic classification of the ISOCP sources, we have started a spectroscopic survey for the 70 unknown ISOCP excess sources ($K_s - LW2 > 2.7$ and $H - K_s > 0.5$). First results obtained at the 1.9 m SAAO telescope by end of January 2004 on ten sources confirm their extragalactic nature (Leipski et al. 2005). The observations reveal two type–1 AGN and two type–2 AGN, one of which (ISOCP08080, Fig. 3.4) has a high [O III] $\lambda 5007$ luminosity above $10^8 L_\odot$ and can be classified as QSO–2. Furthermore, we find two reddened LINER and four extremely reddened emission–line galaxies. Example spectra are given in Fig. 3.4.

The visual extinction of the emission–line galaxies as inferred from the ratio $H_\alpha/H_\beta > 10$ is $A_V \geq 3$ mag; actually A_V is expected to be much stronger when derived from data at longer wavelengths, as found in many dust–enshrouded IR sources (e.g. Haas et al. 2001). The redshift range is $0.1 \leq z \leq 0.5$.

Evidence is growing that LINER galaxies contain an AGN (e.g. Satyapal et al. 2004). Also the four emission–line galaxies may contain an AGN, since their flux ratio F_{60}/F_{LW2}

< 100 is below that found for known pure starburst IR galaxies. Therefore, the ongoing results with a fraction of 40% (4/10) optically identifiable classical AGN are consistent with our prediction that most of the ISOCP excess sources are AGN. Alternatively, we would have to postulate a new population of dust-enshrouded unusually cool star-forming galaxies.

3.4 Conclusions

We have discovered a sample of unique MIR excess sources. Various arguments suggest that they likely contain an AGN. The ongoing optical spectroscopy indicates 40% of the sample to be classical AGN and the remaining part to be dust-enshrouded sources. They appear enigmatic in terms of having a high MIR/NIR flux ratio, but relatively low FIR upper limits. Since a moderate FIR/MIR flux ratio is more typical for AGN, it argues against pure starbursts. This conjecture has to be confirmed. Because of the high extinction, optical observations might not be able to see the true AGN or starburst or composite nature of those sources. Therefore, future observations with XMM-Newton and IR spectroscopy with the Spitzer Space Telescope are planned.

If all 80 ISOCP MIR excess sources turn out to be AGN and if 32 of them (= 40%) are classical AGN which could have been identified also in optical surveys, then the number counts of AGN may increase by a factor of up to $80/32 = 2.5$ due to the inclusion of dusty AGN. Clearly, a reliable comparison will have to wait until spectra of more ISOCP sources are obtained.

The emphasis of this chapter is on presenting a promising strategy how to find the presumed missing AGN. The selection of MIR excess sources via the $H - K_s$ and $K_s - LW2$ colour-colour diagrams in combination with the low $60\mu\text{m}$ upper flux limits turns out to be efficient in separating starbursts from AGN. It will establish a long sought-after technique for selecting the full population of AGN largely free of extinction.

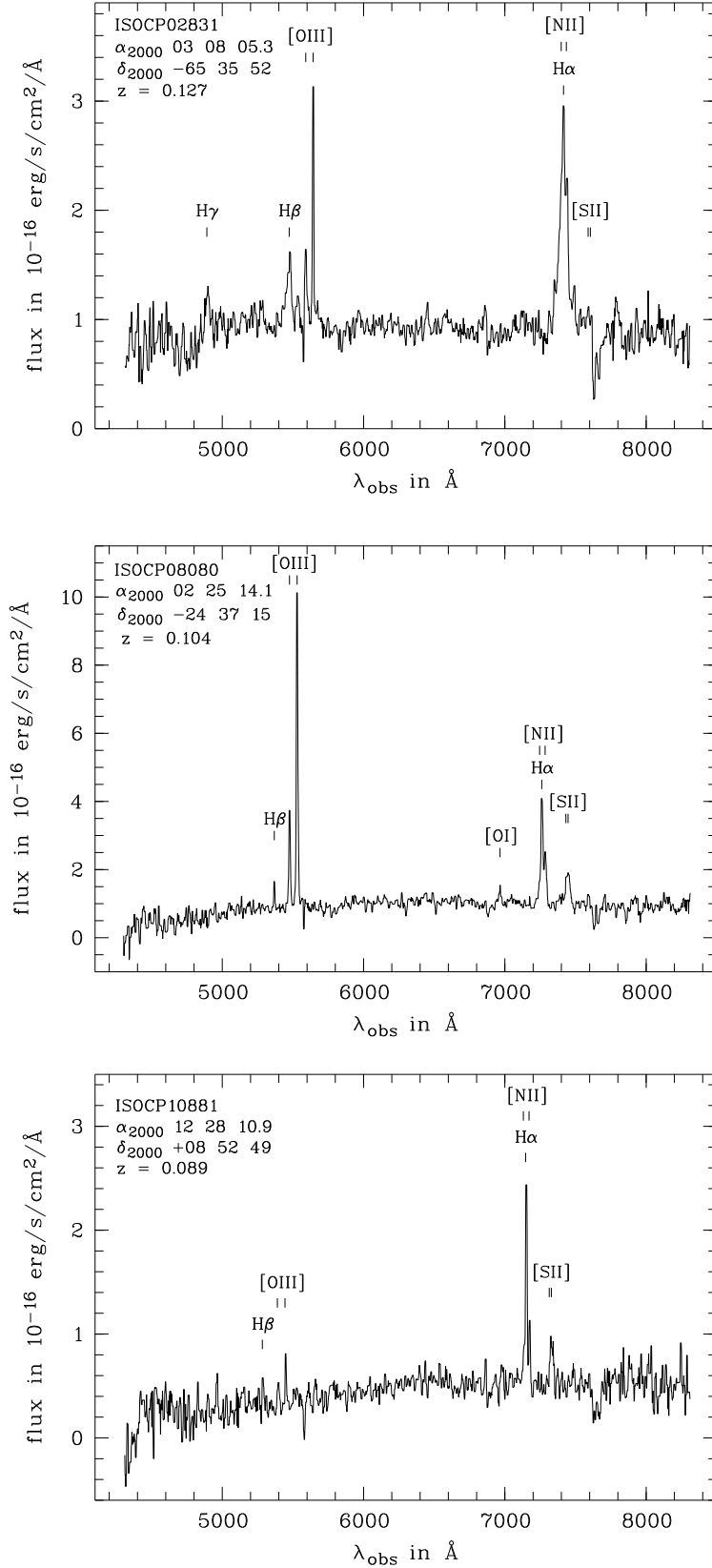


Figure 3.4: Optical spectra of three ISOCP sources with $H - K_s > 0.5$ and $K_s - LW2 > 2.7$ obtained at the SAAO 1.9 m telescope: ISOCP02831: type-1 AGN with broad H α and H β lines, ISOCP08080: type-2 AGN, ISOCP10881: reddened emission line galaxy with $H_\alpha/H_\beta > 10$.

The ISO–2MASS AGN survey: On the type–1 sources

Attempts to overcome the limits by dust extinction in optical AGN surveys and to identify the entire AGN population – including type–2 and buried AGN – encompass surveys in the radio, X–ray and infrared ranges. However, only about 30% of AGN are radio–loud (Urry & Padovani 1995). Hard X–rays enabled the discoveries of elusive AGN completely hidden in starburst nuclei (Maiolino et al. 2003). However, there exists also a significant fraction of X–ray faint AGN (Wilkes et al. 2002), suggesting that also other search techniques should be considered.

The finding of obscured AGN is further complicated by the contribution of the host galaxies, which may dominate the observed properties. Using IRAS $25\ \mu\text{m}/60\ \mu\text{m}$ colours far–IR searches already indicated that the local space density of AGN may be significantly higher than deduced from optical searches (Low et al. 1988).

Among far–IR dominant ULIRGs only few show AGN–typical mid–IR spectral lines (e.g. Armus et al. 2004) or X–ray evidence for powerful buried quasars (Ptak et al. 2003). Searching among the 2MASS survey for very red AGN the extreme $J-K > 2$ colour selection reveals new type–1 AGN at redshifts $z < 0.8$ with moderate luminosities (Cutri et al. 2002).

The FIRST–2MASS study finds about 20% previously overlooked radio–loud quasars not suspicious in the UV (Glikman et al. 2004). Although the contribution of the 2MASS red AGN to the cosmic X–ray background may be as high as 30% (Wilkes et al. 2003), a considerable fraction of the AGN population might still be missed.

The disadvantage of heavy extinction in optical surveys can turn into a valuable detection tool, when observing dust–surrounded AGN at near–infrared (NIR) *and* mid–infrared (MIR) wavelengths. There, the reemission of the dust heated by the strong radiation field of the AGN should be seen as IR excess.

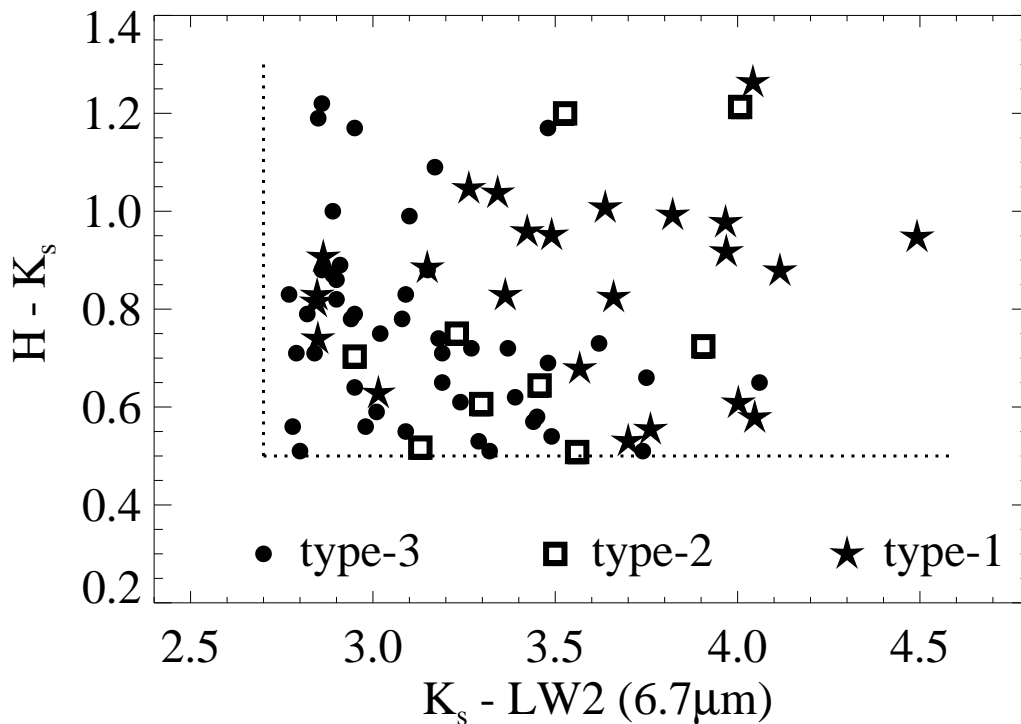


Figure 4.1: IR colour–colour diagram of the ISO–2MASS AGN.

We have started a new approach, searching for AGN by means of their near- and mid-IR emission properties of the putative nuclear dust torus. The *ISOCAM Parallel Mode Survey* “ISOCAP” (Cesarsky et al. 1996; Siebenmorgen et al. 1996; Ott et al. 2003, 2006) provides $6.7\ \mu\text{m}$ data for a large number of extragalactic sources and is therefore an ideal hunting ground for a hitherto unknown population of AGN.

The sample selection and first results from a subsample are described in detail in chapter 3 and by Haas et al. (2004a). Here we report on the results for type–1 AGN from the full sample of those ISOCAP sources which have 2MASS counterparts.

4.1 Results and discussion

4.1.1 Properties of the ISO–2MASS AGN

Within our sample we find 24 broad-line type–1 AGN ($\sim 31\%$, redshift range $z=0.1$ – 2.3), nine narrow-line type–2 AGN ($\sim 12\%$, $z=0.1$ – 0.3), and 44 emission line galaxies with LINER and HII type spectra ($\sim 57\%$, $z=0.03$ – 0.3). None of the objects turned out to be a star. The emission line galaxies, henceforth denoted type–3 sources, are heavily reddened ($H_\alpha/H_\beta > 10$) and their spectra show clear signatures of the host galaxy. Their high MIR/NIR, but low FIR/MIR flux ratio typical for AGN argues against pure

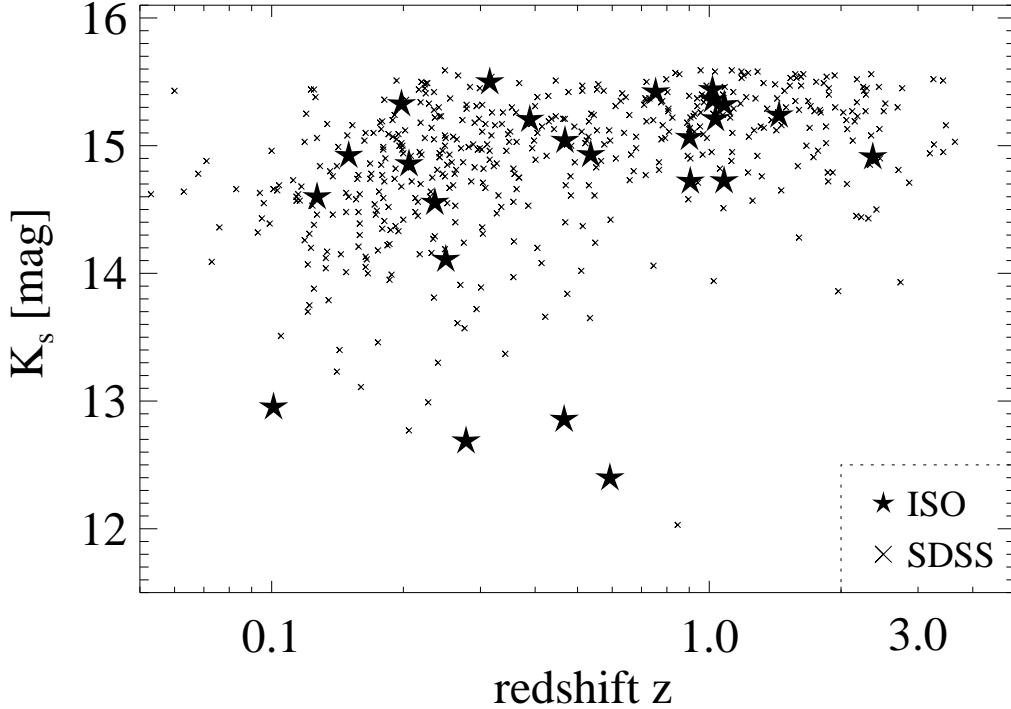


Figure 4.2: Distribution of K_s magnitude and redshift for the ISO–2MASS type–1 AGNs and SDSS–QSOs (only every tenth object plotted).

starbursts. Essentially none of the sources has been detected by IRAS.

The distribution of the different types of sources in the colour–colour diagram is shown in Fig. 4.1. While in $H - K_s$ only minor trends are present, we see a striking dependence in $K_s - LW2$: The type–1 and type–3 sources concentrate toward the right– and left–hand sides, respectively, while type–2 sources are more intermediate. This suggests that we see the hot dust emission best in the type–1 sources, while it is more obscured or intrinsically less prominent in some of the type–2 sources and in most of the type–3 ones. Type–2 and type–3 sources will be investigated in detail in a forthcoming paper. In the following discussion we consider only the type–1 sources and Tab. 4.1 summarises their parameters.

The K_s brightness of the type–1 AGN spans the range $12.4 < K_s < 15.5$. Figure 4.2 shows the distribution of K_s over z . Using a Λ cosmology with $H_0 = 71 \text{ km s}^{-1} \text{ Mpc}^{-1}$, $\Omega_{\text{matter}} = 0.27$ and $\Omega_{\Lambda} = 0.73$ (Bennett et al. 2003), the type–1 sources exhibit an absolute K_s –band magnitude in the range of -25 to -30 , similar to the SDSS quasars. This qualifies them as QSOs, henceforth denoted ISO–2MASS QSOs. In this calculation no k –correction was applied; if done, it would further increase the luminosity of the objects.

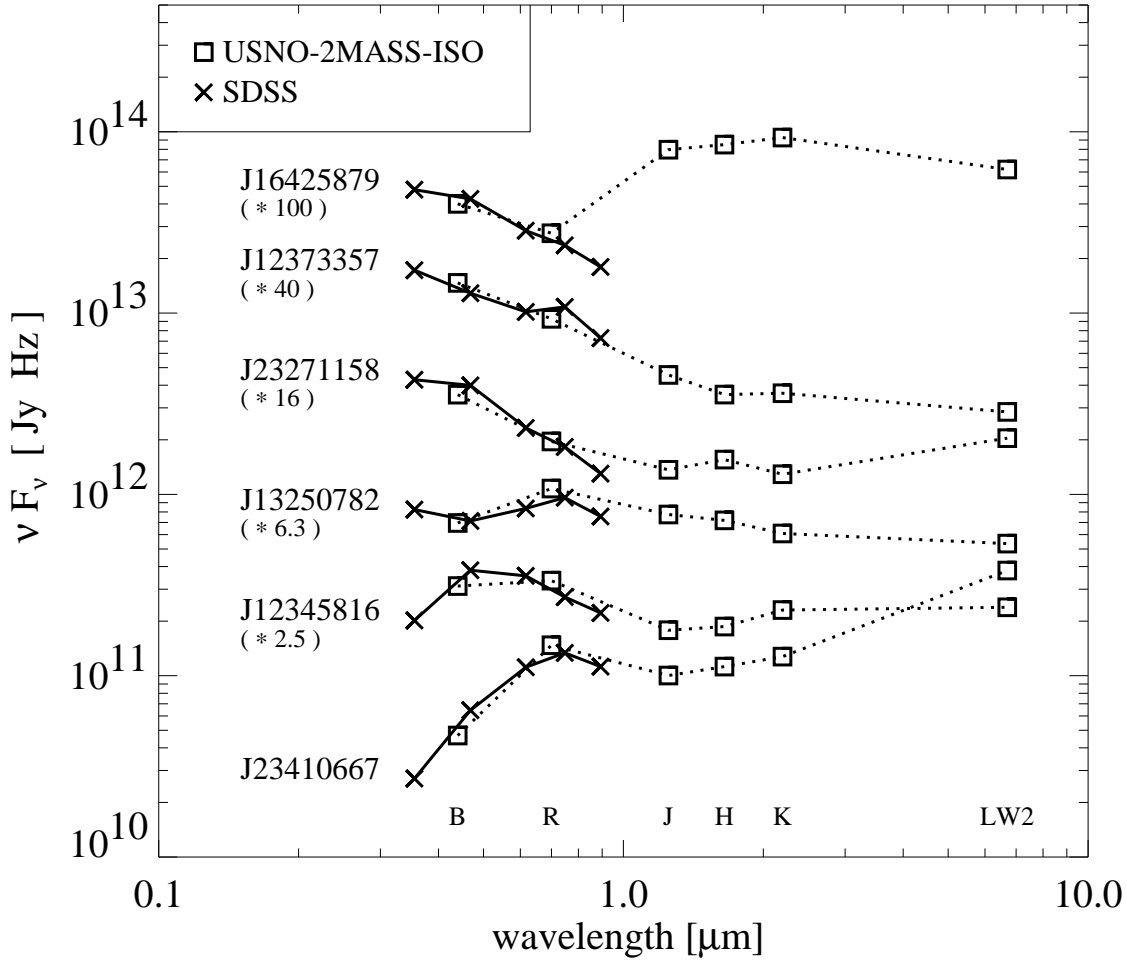


Figure 4.3: SEDs of the six ISO–2MASS QSOs with SDSS photometry. Dotted lines refer to USNO–B photometry and solid lines to SDSS photometry. The good match confirms the USNO data.

Five of the ISO–2MASS QSOs are detected by NVSS or FIRST, three being radio–loud with $F_{1.4\text{GHz}} > F_{2.2\mu\text{m}}$.

Optical B - and R -band photometry of the sources is provided by the USNO catalogue (USNO–B, Monet et al. 2003), with a range of $15.7 < B < 19.7$ and $15.5 < R < 17.9$. We found that the B - and R -band photometry is consistent with that derived from the spectra. The ISO–2MASS AGN span a colour range $-0.4 < B - R < 2.2$; 42% (10/24) have $B - R > 1$. Figure 4.3 shows the MIR to optical spectral energy distributions (SEDs) for those sources for which also SDSS photometry is available. Even the mean SED shows red colours compared to other samples, especially at shorter wavelengths (Fig. 4.4).

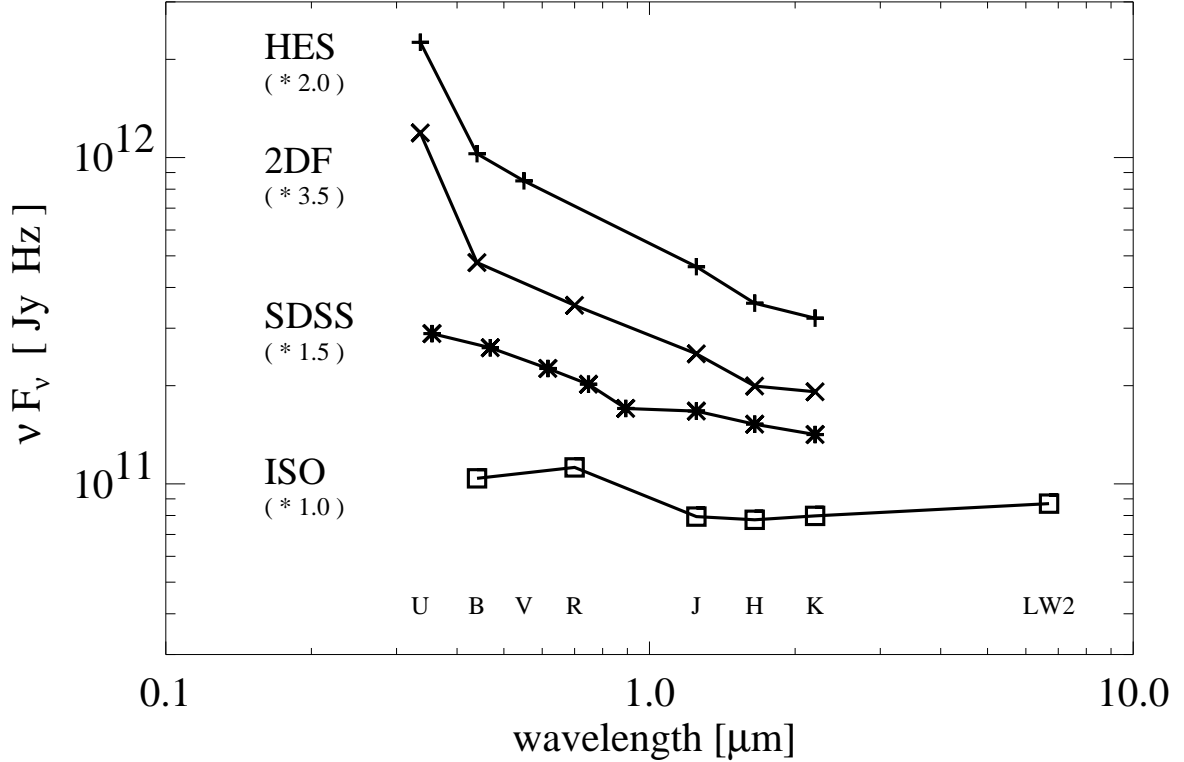


Figure 4.4: Mean SEDs of QSO samples with 2MASS counterparts.

4.1.2 Comparison with optical–UV selected QSOs

If the ISO–2MASS QSOs comprise the same QSO population as that found by optical–UV selected QSO samples, then the number counts as well as the mean SEDs should be similar for suitably matched bins. We compare the ISO–2MASS QSOs with the quasars in the SDSS DR3 (Schneider et al. 2005), the 2QZ+6QZ catalogues of the 2DF survey (Croom et al. 2004), and the Hamburg/ESO quasar survey (HES, Wisotzki et al. 2000). We also correlated these reference catalogues with the 2MASS archive, thereby creating sub-samples hereafter called SDSS–2MASS, 2DF–2MASS, and HES–2MASS, respectively. Fig. 4.2 shows the redshift and K_s -band magnitude distributions of the ISO–2MASS QSOs and the SDSS–2MASS QSOs.

Apart from the low number statistics of the ISO–2MASS QSOs, we find that the redshift and K_s -band magnitude distributions of the ISO–2MASS QSOs and all three optical samples do not differ severely, so that a comparison of the number counts makes sense. However, the SDSS spectroscopy is limited to sources with $i > 15$ (Richards et al. 2002) which translates to $K_s > 13$ (only $\sim 10\%$ of the SDSS–2MASS QSOs have $i - K_s < 2$). Therefore we exclude all objects with $K_s < 13$ in the following discussion.

In order to compare the number of quasars found per deg^2 for the different samples we chose various bins down to the flux limits of the ISO–2MASS QSOs at $R < 18$ and $K_s < 15.5$ and separate also at $z = 0.8$. The USNO photometry yields on average smaller $B - R$ values compared with newer photometric samples, mainly because of differences in the B -band, while the R -band values are more comparable. In order to allow for a more homogeneous photometric comparison, we also used the R -band photometry from USNO for selecting the optical QSO sub-samples (Table 4.2).

The basic results are illustrated in Fig. 4.5. For all reasonable bins the surface density of ISO–2MASS QSOs is by a factor of 1.5 to 10 higher than for the optically selected QSOs. We did not find any reasonable bins to match the surface densities of the IR- and the optically selected QSOs samples.

This result is remarkable as Vanden Berk et al. (2005) report a completeness of 80% to 95% for the SDSS quasar survey. We searched the SDSS DR3 for photometric and spectroscopic data of the 24 ISO–2MASS QSOs. Six have *ugriz* photometry available; compared to the mean SEDs (Fig. 4.4) they show a more or less red SED, even shortward of the B -band (Fig. 4.3). According to the SDSS colour criteria (Richards et al. 2002) two of these six sources lie in the stellar loci and are not foreseen for SDSS spectroscopy, two seem to be potential QSO candidates and two have been identified spectroscopically as QSO. The extrapolation from these six sources indicates that the completion of the SDSS spectroscopy may at most double the optical colour selected number of QSOs, and that one third of the 24 ISO–2MASS QSOs will be missed by the SDSS spectroscopic QSO search due to star-like colours.

Figure 4.4 illustrates that shortward of the R -band the mean SED of the ISO–2MASS QSOs is significantly redder than that of the optically selected QSOs (with 2MASS counterparts), in particular for the 2DF–2MASS and the HES–2MASS QSOs, which show a strong upturn shortward of the B -band. Both results, the higher QSO surface density and the redder SEDs, are independent of the magnitude or NIR colour bins chosen. We conclude that the ISO–2MASS AGN survey discovers a QSO population, about a third of which is clearly different from that found in the optical surveys.

On the other hand, down to $R < 18$ the 2DF and SDSS QSO surveys find about 40-50% blue QSOs which have $K_s > 15.5$, hence are fainter than the detection limit of the ISO–2MASS survey; these optical QSOs without 2MASS counterpart have on average bluer optical colours than those with 2MASS counterparts.¹ To get an estimate of the entire IR- and optical QSO number counts down to $R < 18$ we add the surface density of ISO–2MASS and SDSS QSOs and subtract the intersection of both samples, i.e. those SDSS quasars that also fulfill our IR selection criteria ($R < 18$ & $13 < K_s < 15.5$ & $H - K_s > 0.5$). Referring to columns 6 and 8 of Tab. 4.2 this corresponds to $\frac{20}{10} + \frac{5669}{4188} - \frac{2685}{4188} \approx 2.7 \text{ deg}^{-2}$ ($\sim 1.5 \text{ deg}^{-2}$ for $z > 0.8$, respectively), i.e. about a factor 2 higher than inferred from the SDSS QSO survey alone.

¹ Notably, the ISOCAM Parallel Survey reveals numerous (>100) $R > 18$ sources without 2MASS counterpart, which are not considered here. Their NIR and optical investigation is still ongoing.

2MASS	$F_{6.7\mu\text{m}}$ [mJy]	redshift	remarks
		z & type from this work	
J01363451+4112497	1.21	0.198	
J03005029−7938450	3.53	0.901	
J03080561−6535520	1.79	0.127	
J11323474−1952448	1.65	0.389	
J11353051−1425344	1.94	0.536	$J-K_s > 2$
J13250782+0541052	1.65	0.206	SDSS phot+spec
J13474549−0841059	1.43	0.754	
J14265292+3323231	2.59	1.083	
J16413748+6541140	1.60	1.082	
J17075650+5630136	1.75	1.019	
J17175947+4956261	2.07	1.018	
J20145083−2710429	2.44	1.444	
J22484115−5109532	16.90	0.101	
J23271158+0114469	3.46	0.468	SDSS phot
J23324586−1414242	2.51	0.315	
J23410667−0914327	8.49	0.236	SDSS phot
		z & type from NED	
J00300421−2842259	31.35	0.278	RQ, $J-K_s > 2$
J01020053−3018259	2.24	1.033	RL
J12345816+1308549	2.12	2.364	SDSS phot
J12373357+1319063	1.33	0.150	SDSS phot
J14590760+7140199	3.11	0.905	RL (3C 309.1)
J15520240+2014016	5.09	0.250	
J16425879+3948369	13.82	0.593	RL (3C 345) SDSS phot+spec
J21145258+0607423	25.04	0.466	RQ

Table 4.1: Parameters of the ISO–2MASS type–1 QSOs. The first 16 sources have been studied for the first time. For the last eight sources the information on source type and redshift was provided by NED. Objects with information from SDSS available are marked.

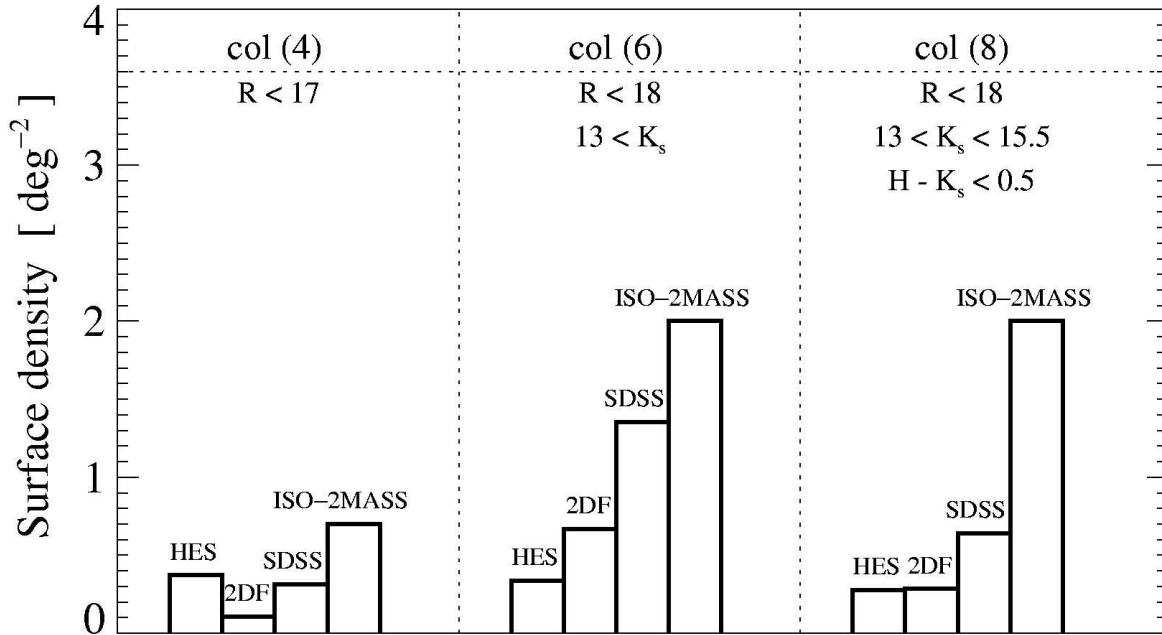


Figure 4.5: QSO number counts of the ISO–2MASS and three optical surveys at three different bins. The column enumeration refers to Tab. 4.2.

The fact that IR counts essentially add to the quasar surface density can most likely be ascribed to quasars (extended as well as pointlike objects) that have stellar colours. Remarkably, in the completeness test of the SDSS QSO survey by Vanden Berk et al. (2005) this population of quasars has largely been excluded. However our data show that these quasars with optical stellar–like colours comprise a considerable fraction of the total population of quasars and that they can efficiently be discovered by IR colours.

4.1.3 Comparison with the 2MASS red AGN survey

Using the colour selection $J - K_s > 2$ the 2MASS red AGN survey found an extrapolated surface density of ~ 0.57 type–1 and type–2 AGN per deg^2 (Cutri et al. 2002), which become lower based on newer larger data sets (R. Cutri, priv. comm.). Two type–1 and two type–2 ISO–2MASS AGN match the criterion $J - K_s > 2$, resulting in $4 / 10 = 0.40$ AGN per deg^2 , roughly comparable to the 2MASS red AGN estimates. Thus the 2MASS red AGN are a proper subset of the ISO–2MASS AGN survey, as expected.

Due to k -correction effects the 2MASS red AGN survey is biased against sources with redshifts $z > 0.8$, hence against high luminosity sources (Cutri et al. 2002). Using a moderate colour criterion $H - K_s > 0.5$ (roughly corresponding to $J - K_s > 1.2$ as used by Francis et al. (2004) the ISO–2MASS AGN survey in fact finds nine (out of 24)

QSOs with $z > 0.8$. As a consequence the ISO-2MASS-QSOs reach by one to three magnitudes higher K_s band luminosities.

4.2 The nature of the ISO-2MASS type-1 QSOs

We combined the ISO 6.7 μm and 2MASS surveys in order to obtain a powerful tool to search for AGN independent of dust extinction. Using moderate colour criteria $H - K_s > 0.5$ and $K_s - LW2 > 2.7$ we have selected a sample of 77 AGN candidates in an effective area of ~ 10 square degrees.

By means of optical spectroscopy we find 24 ($\sim 30\%$) type-1 QSOs at redshifts $0.1 < z < 2.3$; nine of them have $z > 0.8$. Part of them have colour properties similar to optically selected QSOs, but about 30% of them have red optical SEDs similar to stars, so that they are missed in optical and UV AGN surveys like SDSS, 2DF, or HES.

With a surface density of about 2 deg^{-2} down to $R < 18$ mag the ISO-2MASS QSOs outnumber the 1.35 deg^{-2} of the SDSS quasar survey by 50%; we find a combined optical-IR QSO surface density of 2.7 deg^{-2} . Since only two of the ISO-2MASS QSOs have also $J - K_s > 2$, the inclusion of the ISO mid-infrared photometry significantly extends the capabilities of the pure 2MASS red AGN survey.

In the framework of a quasar's evolution from an initially dust-enshrouded object to a clean one (Sanders et al. 1988; Haas et al. 2003) we suggest that the red objects comprise young members of the QSOs population. If true, then the high (about 30%) fraction of these young objects indicates that the QSOs spend much of their life time in a dust surrounded phase, before they change their appearance becoming optically blue. Future studies may provide further clues to this issue as well as their contribution to the X-ray background.

(1) Sample	(2) area deg ²	(3) total N	(4) number (N) and surface density N/area (deg ⁻²) of quasars with									
			$R < 17$		$R < 18$		$R < 18$ $K_s > 13$		$R < 18$ $13 < K_s < 15.5$		$R < 18$ $13 < K_s < 15.5$ $H - K_s > 0.5$	
			N	deg ⁻²	N	deg ⁻²	N	deg ⁻²	N	deg ⁻²	N	deg ⁻²
<i>R</i> -band photometry from USNO												
ISO-2MASS												
$z > 0.0$	~10	24	7	0.7	24	2.4	20	2.0	20	2.0	20	2.0
$z > 0.8$	~10	9	1	0.1	9	0.9	9	0.9	9	0.9	9	0.9
HES												
$B < 17$	>1000	415	371	<0.37	415	<0.42	337	< 0.34	336	<0.34	277	< 0.28
$B < 17$ and $z > 0.8$	>1000	140	122	<0.12	140	<0.14	137	< 0.14	137	<0.14	84	< 0.08
SDSS DR3												
$z > 0.0$	4188	44298	1309	0.31	5713	1.36	5669	1.35	3149	0.75	2685	0.64
$z > 0.8$	4188	35459	497	0.12	3303	0.79	3303	0.79	1213	0.29	846	0.20
2DF 2QZ+6QZ												
$z > 0.0$	721.6	19304	76	0.11	484	0.67	483	0.67	253	0.35	205	0.28
$z > 0.8$	721.6	16055	41	0.06	320	0.44	320	0.44	143	0.20	92	0.13
<i>R</i> -band photometry from SDSS and 2DF, respectively												
SDSS DR3												
$z > 0.0$	4188	46420	568	0.14	4700	1.13	4657	1.11	2653	0.63	2212	0.53
$z > 0.8$	4188	37322	300	0.07	3068	0.73	3068	0.73	1285	0.31	901	0.22
2DF 2QZ+6QZ												
$z > 0.0$	721.6	23660	62	0.09	727	1.01	726	1.01	327	0.45	271	0.38
$z > 0.8$	721.6	19775	32	0.04	486	0.67	486	0.67	161	0.22	115	0.46

Table 4.2: Number counts of the IR and optical QSO samples for various bins. We adopt Poisson errors (\sqrt{N}) for the ISO-2MASS QSO sample. In the upper four blocks of the table we use the *R*-band photometry from the USNO catalog, in the lower two ones the *R*-band photometry is from 2DF and SDSS themselves (for SDSS: $R = g' - 1.14(g' - r') - 0.14$ according to Smith et al. (2002)).

The reddest ISO–2MASS quasar

Pure optical quasar surveys only find QSOs with essentially blue continua (e.g. Schmidt & Green 1983; Wolf 2005). However, investigations including the radio, X–ray and infrared have revealed a substantial fraction of dust–reddened AGN missed by optical surveys (Glikman et al. 2004; Maiolino et al. 2003; Low et al. 1988). We have combined the ISOCAM Parallel Survey at $6.7 \mu\text{m}$ with the 2MASS survey in order to obtain a powerful tool to search for AGN (Haas et al. 2004a). In fact, in a high galactic latitude area of 10 deg^2 we found 30% more type–1 quasars per square degree down to $R=18$ mag than e.g. the SDSS DR3 quasar survey (Leipski et al. 2005).

The quasars found by our NIR/MIR method show a variety of spectral shapes, in particular in the optical. Some of the ISO–2MASS objects are too red to be recognised as quasars by current optical strategies, probably because of dust extinction. Since the NIR and MIR colours of quasars are different from those of stars, selection in the infrared enables the detection of optically red quasars (Smith et al. 2003; Leipski et al. 2005). Also other MIR searches have been started using the Spitzer Space Telescope finding a large number of quasars, but the fraction and the properties of red AGN in these searches has still to be explored (e.g. Lacy et al. 2004a).

The most interesting object among the 24 QSOs discovered by the ISO–2MASS survey is a red broad–line quasar at $z = 0.236$ (2MASS J23410667–0914327, hereafter called J2341). Alternatively to the classical $M_B < -23$ quasar definition, its K_s –band luminosity $M_{K_s} = -25.8$ qualifies J2341 as a quasar. While no radio counterpart is listed by SIMBAD, ROSAT HRI observations give a soft X–ray luminosity of $L_{0.5-2.4 \text{ keV}} \sim 3 \times 10^{43} \text{ erg s}^{-1}$, similar to that of low redshift PG–quasars.

5.1 Results and Discussion

The R –band acquisition image reveals a faint object near J2341 approximately $1''.8$ north–west of the quasar (Fig. 5.1, position angle $\sim 294 \text{ deg}$), which could be a physically interacting companion galaxy. Therefore, we oriented the slit for the VLT spectroscopy

Ion	λ_{rest}	flux $10^{-15} \frac{\text{erg}}{\text{s cm}^2}$	luminosity $10^{41} \frac{\text{erg}}{\text{s}}$
[Ne v]	3426 Å	0.193	0.32
[O II]	3727 Å	0.196	0.32
[Ne III]	3967 Å	0.110	0.18
[O III]	5007 Å	1.911	3.13
[Ne II]	12.8 μm	3.967	6.50
[O IV]	25.9 μm	4.683	7.67

Table 5.1: Line fluxes and luminosities of narrow emission lines in J2341. The luminosities were calculated with a luminosity distance of 1169.95 Mpc as determined using recent WMAP cosmology (Bennett et al. 2003); $H_0 = 71 \text{ km s}^{-1}$, $\Omega_{\text{matter}} = 0.27$, and $\Omega_{\Lambda} = 0.73$.

along both objects to determine type and redshift of the companion.

Because this double object is not resolved by 2MASS additional NIR imaging was performed to obtain photometry for both sources separately (see chapter 2).

The optical spectroscopy reveals that both objects have the same redshift ($z = 0.236$). The separation of $1''.8$ ($\sim 6.7 \text{ kpc}$) suggests that the two objects are interacting. No clear evidence for an interaction (e.g. morphological peculiarities or tidal tails) can be seen on the acquisition frames (R -band; 30 sec integration time).

However, close visual inspection reveals that both objects are embedded in weak diffuse emission. In the following, the name “J2341” will refer to the quasar while the secondary object is called companion.

5.1.1 The quasar

The spectrum of J2341 shows prominent broad emission lines (FWHM $\sim 2800 \text{ km/s}$) on top of a red continuum (Fig. 5.1). This is unusual for type–1 AGN. In Fig. 5.2 we plot the mean SDSS quasar template (VandenBerk et al. 2001) over the spectrum of J2341¹. While J2341 agrees with the optical quasar template longwards of $\sim 5000 \text{ Å}$, the difference is obvious at shorter wavelengths. The optical continuum of J2341 is significantly redder and the discrepancy increases shortwards of $\sim 5000 \text{ Å}$ where the continuum of classical quasars is blue and dominated by power–law like continuum emission.

J2341 is also significantly redder than the reddened quasars found using optical multi–colour selection techniques (e.g. Richards et al. 2003). However, the flux ratio of the broad Balmer emission lines is approximately the same for J2341 and for the template, indicating that the BLR of J2341 is not reddened. We discuss this issue further in § 5.1.4.

¹ We scaled both spectra to match in $\text{H}\alpha$. If substantial absorption is present towards the broad–line region (BLR) it is very likely that also $\text{H}\alpha$ is partly obscured and then the applied scaling might be misleading. However, the main trends would be conserved.

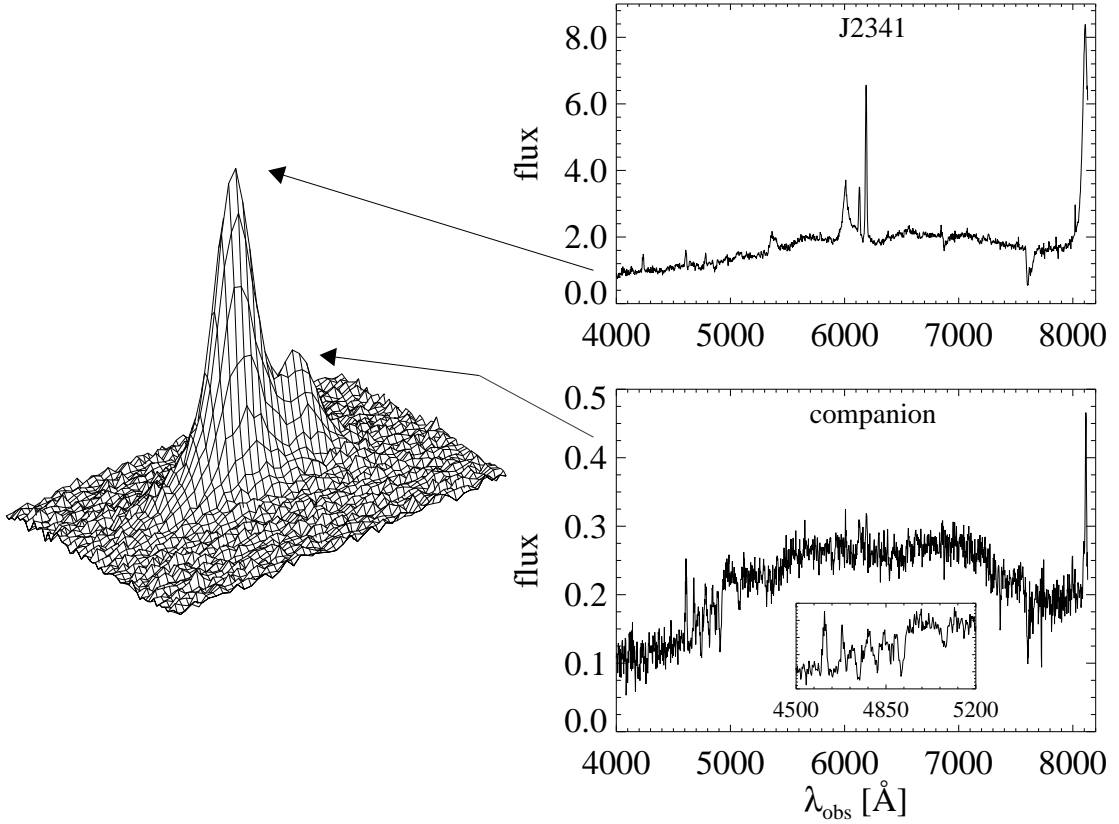


Figure 5.1: Surface plot of the R-band acquisition image of J2341 and spectra of the two objects. The inset in the companion spectrum enlarges the stellar absorption features. Fluxes are given in $10^{-17} \text{ erg s}^{-1} \text{ cm}^{-2} \text{ \AA}^{-1}$.

Fig. 5.3 shows an enlarged view of the blue portion of the quasar spectrum. Broad Balmer emission lines and considerable Fe II emission are detected, as well as high and low ionisation forbidden lines from the narrow-line region (e.g. [Ne V], [O II], [Ne III], [O III]; Tab. 5.1). We also detect Ca II K and possibly CN as absorption features from the host galaxy. The presence of Ca II K without higher order Balmer absorption suggests that J2341 does not have a strong contribution from a young-to-intermediate age stellar population.

For the MIR spectroscopy, the slit sizes of the IRS observations include both objects but the spectrum is likely to be dominated by emission from the quasar, which is four times brighter at K_s than the companion. The MIR spectrum shows only few features and is dominated by the strong power-law continuum known from classical AGN (e.g. Weedman et al. 2005; Ogle et al. 2006; Buchanan et al. 2006) (Fig. 5.4). We clearly detect emission lines like [O IV] and [Ne II] (Tab. 5.1). The high ionisation [Ne V] lines, although prominent in the optical spectrum (Fig. 5.3) are only marginally detected. The

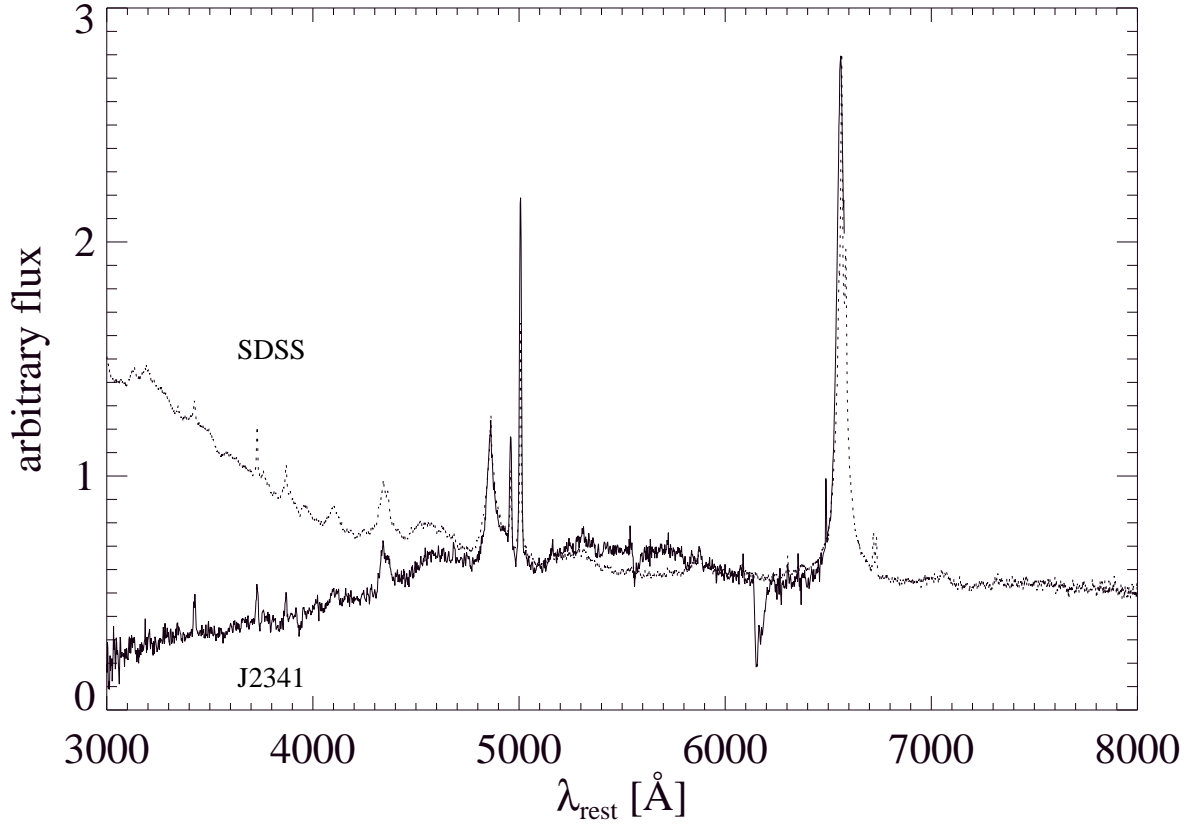


Figure 5.2: Comparison of J2341 with the mean SDSS quasar template of Vanden Berk et al. (2001). The spectra were scaled to match in $H\alpha$.

MIR spectrum shows neither PAH emission nor silicate absorption. The latter indicates that the source of the dust continuum emission is not considerably obscured at MIR wavelengths, as further discussed in § 5.1.4. This places constraints on the distribution and column density of any obscuring material that reddens the optical continuum source.

In Fig. 5.2 we additionally plot the IRS spectrum of the broad–line AGN/ULIRG Mrk 231. In contrast to J2341, Mrk 231 shows silicate absorption, although broad permitted lines are present in its optical spectrum, i.e. the inner regions of its AGN are visible. In J2341 on the other hand, it seems that there is not enough dust lying between the torus and the observer to produce significant silicate absorption.

This is consistent with the optical results where the NLR and the BLR do not show signs for strong dust reddening. Mrk 231 also exhibits a significant FIR bump that indicates powerful hidden starbursts. Since J2341 has relatively low FIR emission, dusty starbursts are not present, as also indicated by the optical spectrum.

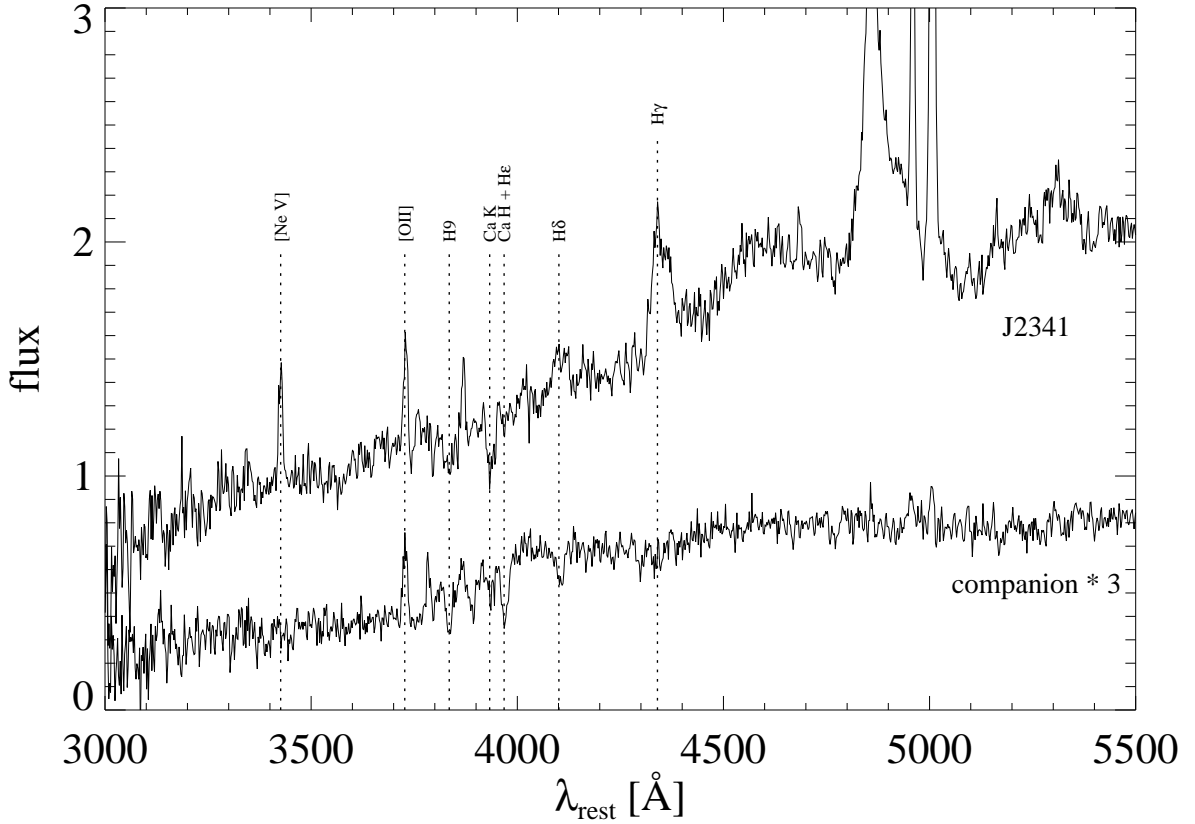


Figure 5.3: Blue portion of the spectra of the quasar and its companion. Important emission and absorption lines are labelled. The spectrum of the companion was scaled by a factor of three to facilitate the comparison. Fluxes are given in $10^{-17} \text{ erg s}^{-1} \text{ cm}^{-2} \text{ \AA}^{-1}$.

In the optical spectrum we detect features of the host galaxy (Fig. 5.3). Since the optical continuum source is suppressed (or absent) while the features of the host galaxy are visible, we conclude that any obscuring dust is concentrated towards the central regions of the galaxy. Additionally, the emission lines from the NLR (e.g. [Ne V], [O II], [Ne III]) have approximately the same strength in J2341 as in unobscured quasars (Fig. 5.2). However, the continuum emission underneath the NLR emission lines is significantly lower, indicating that the NLR suffers far less obscuration than the continuum. Therefore, the mayor part of the obscuring material (if present at all) seems to be located in the very centre between the NLR and the accretion disc.

One would expect that such a scenario triggers enhanced nuclear star formation. To study the rate of star formation in quasars, Ho (2005) examined the [O II]/[O III] flux ratio of PG quasars. Low ratios between 10% and 30% are consistent with pure AGN origin. Using this method for J2341 the low [O II]/[O III] ratio of $\approx 10\%$ does not indicate strong starbursts (Tab. 5.1).

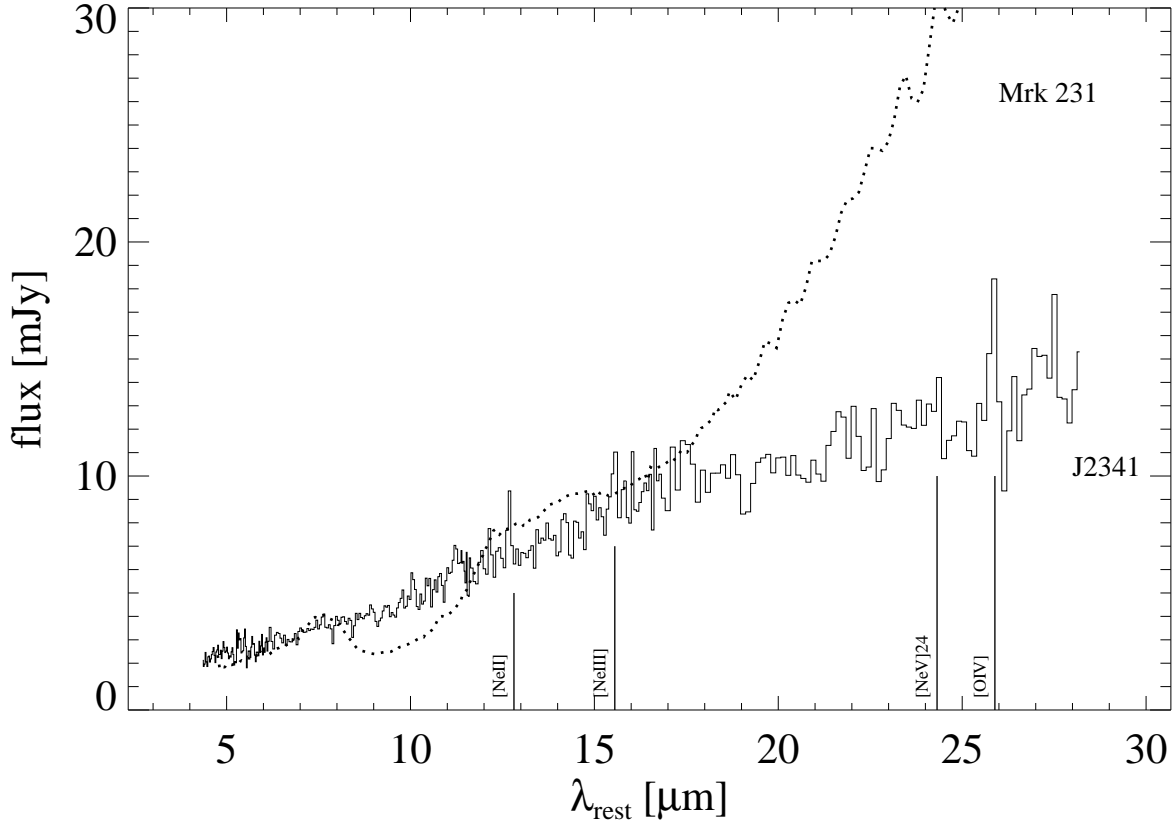


Figure 5.4: IRS/Spitzer spectrum of J2341. The continuum and a few strong emission lines are detected. The IRS spectrum of the AGN/ULIRG Mrk 231 is shown as a dashed line (Weedman et al. 2005).

5.1.2 The companion

The optical spectroscopy of the object near J2341 yields a redshift similar to that of the quasar (Fig. 5.1). Considering the small angular separation of $\sim 1''.8$ (~ 6.7 kpc projected linear separation) both objects are likely interacting. The spectrum of the companion is reminiscent of an E+A galaxy with additional ongoing star formation traced by significant [O II] emission (Fig. 5.3).

The presence of an intermediate age population (few hundred megayears) in the companion may be an indication that the interaction has initiated a burst of star formation in the past. However, the evolving system still leads to ongoing star formation at moderate levels.

5.1.3 Comparison with other red quasars

The new NIR photometry provides J , H , and K_s magnitudes for J2341 and its companion individually (see chapter 2). Additionally, we determined the R band magnitudes from

Filter	quasar	companion	sum	2MASS ^a	2MASS ^b
<i>R</i>	18.186	20.148	18.021	17.52 ^c	–
<i>J</i>	16.119	18.560	16.010	16.505	16.065
<i>H</i>	15.327	17.687	15.210	15.502	15.234
<i>K_s</i>	14.600	17.073	14.494	14.555	14.577

Table 5.2: Photometry of the J2341 system, given in Vega magnitudes. The errors of the NIR photometry are ≤ 0.1 mag.

^a Default 2MASS photometry includes both objects.

^b 2MASS 4'' aperture photometry.

^c *R*-mag taken from USNO-B.

the acquisition images. Inspection of Tab. 5.2 reveals that for our slightly extended object some flux is missed when measured via the (default) point-source photometry of 2MASS. More appropriate is the 2MASS aperture photometry (aperture 4'') that includes both objects. It agrees well with our new photometry which reduces the $J - K_s$ colour of the quasar from 1.95 to ~ 1.5 (Tab. 5.2). J2341 and the companion have the same NIR colours within the measurement errors.

If both objects have a strong contribution of an old stellar population (as indicated by the spectra), the $R - K_s$ colour should be the same for both hosts. However, the $R - K_s$ colour of the quasar is redder by 0.5 mag. Then the difference of 0.5 mag may be attributed to additional AGN related hot dust in the quasar. Assuming that *R* is dominated by host galaxy emission, the $R - K_s$ colour difference translates roughly to an amount of 50% that is contributed by AGN related dust emission in the K_s band.

The NIR colours of J2341 are bluer than the $J - K_s$ colour used to select the red 2MASS AGN (Cutri et al. 2002). As well as NMIR searches, the 2MASS red AGN find objects with various optical continuum slopes (e.g. Smith et al. 2003; Leipski et al. 2005) and also with various X-ray properties (e.g. Wilkes et al. 2002). For the red 2MASS AGN we most likely observe a mixture of essentially unobscured sources and absorbed sources. The red NIR colours can then be attributed to either clearly visible emission from hot dust in the centre or to absorption of the NIR continuum by more diffuse dust.

J2341 clearly shows a spectroscopically confirmed companion (Fig. 5.1), but this is not generally the case among the red 2MASS AGN. While on HST images a number of these quasars show companions and signs for interaction, the fraction of such objects is about the same as for the blue, UV-selected PG quasars (Marble et al. 2003). In the picture where nuclear activity is triggered by interaction, quasars are usually thought to be late stages of a merger event. The early stage may have been a ULIRG. Red quasars are then supposed to represent young members of the QSO population at intermediate evolutionary stages. However, while almost all ULIRGs show signs for interaction red quasars as well as classical blue ones only do for a small fraction ($\sim 30\%$, Marble et al. 2003).

5.1.4 The nature of J2341

We now discuss some scenarios in order to explain the low continuum emission of J2341, while the BLR and NLR appear essentially absorption free. In this case either the optical continuum from the accretion disk is intrinsically present but absorbed or it is even missing.

In the latter case J2341 may harbour a radiatively inefficient accretion flow (RIAF). However, RIAFs are usually successfully attributed to low-ionisation objects and we detect significant emission of elements with high ionisation ([O III], [Ne V]). Alternatively, in the case of absorption the dust may be distributed in a torus which is moderately inclined, so that a part of the BLR is seen, but the accretion disk is completely hidden. Then the torus must have a rather sharp edge, a requirement which looks somewhat unlikely. More severely, the MIR spectra show essentially no silicate absorption, placing a limit on the optical absorption ($A_V < 1$). Additionally, the presence of the interacting companion of J2341 favours a disturbed dust distribution with a sharp torus edge being somewhat unlikely.

Another possible explanation is that the dust is distributed in clumps located inside the BLR, and dust clouds lie by chance in our line of sight towards the accretion disk. This reddens the continuum emission from the centre, while the rest of the BLR is not affected by dust clouds. But also the last option is not free of objections, since it requires a special geometry and, moreover, the dust has to be located very near to the continuum source where the strong radiation field may destroy the dust particles. However, in support of our findings the presence of a compact absorber very near to the active nucleus was already proposed to explain results from X-ray spectroscopy of red AGN where the BLR is visible but the X-ray source is obscured (Wilkes et al. 2005).

Additional observations like spectropolarimetry or X-ray spectroscopy may provide further clues on the nature of J2341, but solving this problem is still a difficult task.

5.2 Conclusions

While there is growing consensus on the existence of numerous dust-enshrouded red quasars, their discovery and detailed exploration is still an observational challenge. Here, we report on a detailed case study of the reddest type-1 quasar of our sample, at redshift $z = 0.236$. Remarkably, on the optical and NIR images we find a star forming emission-line galaxy at the same redshift of J2341 with a projected separation of $1''.8$ (6.7 kpc).

The mid-infrared spectrum shows low- and high-excitation emission-lines superimposed on a power-law spectral energy distribution typically seen in type-1 quasars. However, the lack of strong far-infrared emission suggests that J2341 is in a stage different from ULIRG-AGN.

The optical spectrum shows no clear signatures for reddening in the emission-lines, while the continuum emission of the active nucleus appears highly absorbed.

While so far the observations of many red 2MASS-AGN with $J - K > 2$ did not find evidence for a triggering companion, we suggest that the dust enshrouded quasar

activity of J2341 is in fact caused by interaction with its companion. The total amount of obscuring dust seems to be relatively small and not widely spread, but concentrated within the BLR.

Narrow-line AGN in the ISO-2MASS Survey

A long-standing challenge of observational AGN research is to find type-2 quasars, the luminous analogs of Seyfert-2 galaxies. According to the AGN unification scheme they are misaligned type-1 quasars, so that the central powerhouse is hidden behind a dusty torus seen edge-on. While among radio loud AGN recent Spitzer spectroscopy could show that the powerful FR II radio galaxies in fact contain quasar-like nuclei (Haas et al. 2005), the detection of radio-quiet type-2 quasars requires other strategies. Hard X-ray surveys turned out to be successful (Norman et al. 2002), but may also be hampered by considerable extinction (Vignali et al. 2004). In the optical using the Sloan Digital Sky Survey type-2 quasars have been found in galaxies with narrow permitted emission lines and high $[\text{O III}]\lambda 5007$ equivalent widths (Zakamska et al. 2003) and were confirmed by spectropolarimetry (Zakamska et al. 2005).

An alternative approach is to look for sources exhibiting the characteristic near- and mid-infrared reemission of the hiding dust which is heated by the strong radiation field of the AGN. While several such AGN searches are ongoing using $3.6 - 8.0 \mu\text{m}$ data obtained by the Spitzer Space Telescope (e.g. Lacy et al. 2004a), we have invented the ISO-2MASS AGN survey at H , K_s , and $LW2$ ($6.7 \mu\text{m}$). The details of the ISO-2MASS sample selection are described by Haas et al. (2004a). We completed the optical spectroscopy and in fact found type-2 AGN in addition to type-1s. The results on the type-1 AGN are presented in chapter 4 and by Leipski et al. (2005). Here, we report about the type-2 AGN.

6.1 Type-2 candidates

The type-2 AGN were distinguished from the emission-line galaxies in the diagnostic line-ratio diagrams of Veilleux & Osterbrock (1987), using the dividing lines from Kewley et al. (2001). This procedure yields eight type-2 AGN (Tab. 6.1). Three of the type-2 objects can be regarded as type-2 QSOs with $[\text{O III}]$ luminosities greater than $3 \cdot 10^8 L_\odot$ (according to the criterion of Zakamska et al. 2003).

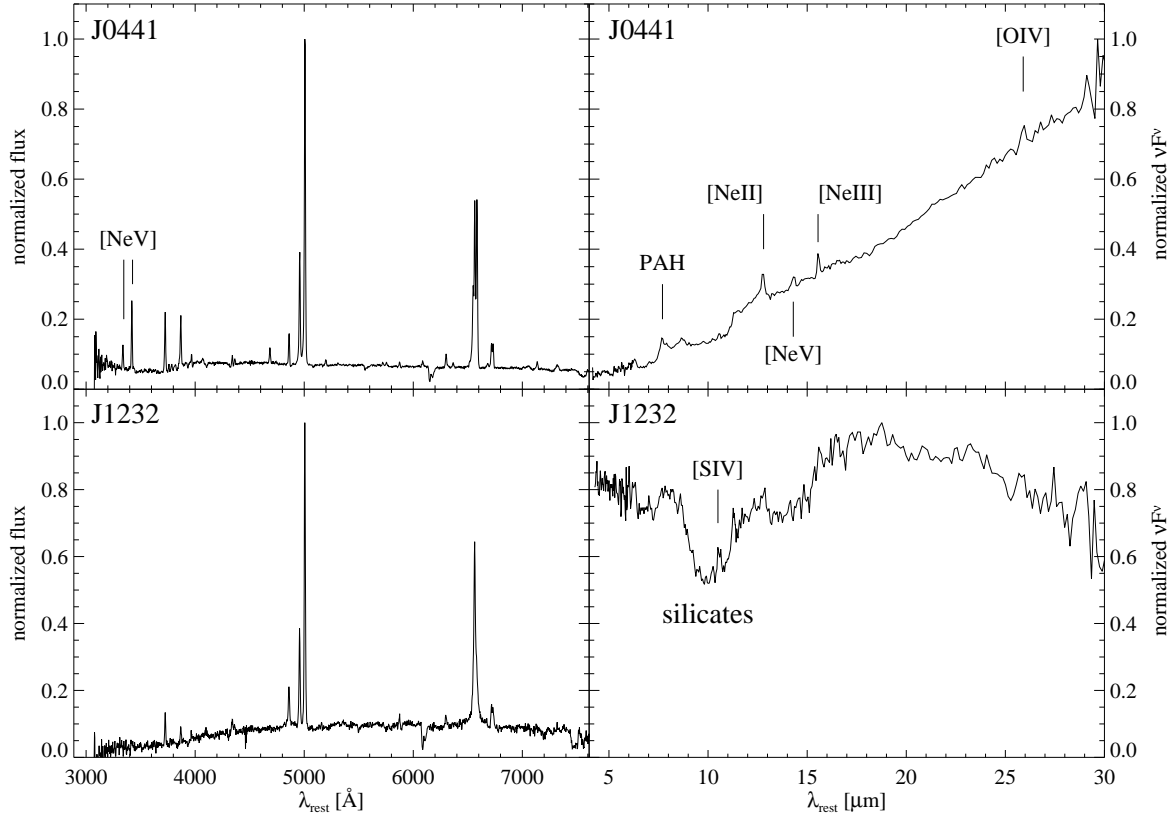


Figure 6.1: Optical (*left*) and MIR (*right*) spectra of two ISO-2MASS type-2 AGN. The individual spectra have been normalised to their peak value. Note that the optical spectra are plotted in a linear flux scale, while the MIR spectra are shown as νF_ν .

6.2 Results and Discussion

The type-2 AGN found by the ISO-2MASS AGN survey show a wide range of properties. In the following we discuss two type-2 objects in detail for which optical as well as MIR spectroscopy is available (J04411405-3734369, hereafter called J0441 and J12324114+1112587, hereafter called J1232). The features of these sources are representative for those found in the other objects. Both type-2 AGN show the prominent optical emission lines from the narrow-line region (NLR), but the features of the host galaxies are different.

6.2.1 J0441

The optical spectrum of J0441 (Fig. 6.1, *upper left*) shows a blue continuum with prominent optical emission lines. The emission lines include e.g. strong [NeV] emission, what is commonly used as a tracer for an active nucleus. Besides the emission lines, the spectrum of J0441 clearly shows absorption lines, especially prominent higher order

2MASS (J2000.0)	$F_{6.7\mu\text{m}}$ mJy	redshift	$L_{[\text{O III}]}$ in $10^8 L_{\odot}$	$L_{[\text{O II}]}$ in $10^8 L_{\odot}$
J04411405–3734369	3.96	0.209	6.34	1.16
J11095861–3720374	2.00	0.173	0.43	0.09
J22090602–3257505	1.92	0.425	21.28	4.98
J02251432–2437154	2.92	0.104	0.40	–
J14563296–0847490	1.69	0.079	0.05	0.02
J12324114+1112587	7.12	0.249	1.75	0.22
J01520465+2232015	0.89	0.113	0.17	–
J19110553+6742507	3.73	0.171	13.93	–

Table 6.1: Parameters of the ISO–2MASS type–2 AGN.

Balmer absorption. The spectrum is reminiscent of a strong contribution of a moderately young (few hundred megayears) stellar population. This young population is superposed on an older population (indicated by the presence of absorption features like Ca II K; Fig. 6.2). That star formation is still ongoing is supported by the strong far–infrared (FIR) emission visible in the Spitzer MIR spectrum (Fig. 6.1, *upper right*). The star formation is also indicated by the presence of PAH emission. This emission, although clearly detected, is of low equivalent width due to a strong NIR and MIR continuum emission caused by the AGN.

Comparing the MIR spectrum of J0441 with the ISO–SWS spectrum of the starburst galaxy M 82, J0441 has redder colours below 20 μm (i.e. a steeper continuum slope) and approximately the same slope at wavelengths greater than 20 μm (Fig. 6.3). Moreover, the strength of the PAH features is much greater in M 82.

Compared with the Spitzer/IRS spectrum of the type–2 AGN/ULIRG Mrk 273 we see that Mrk 273 has intermediate PAH strength and a very steep slope towards FIR wavelengths, most likely due to vigorous starbursts (Fig. 6.3).

J0441 is one of the very few ISO–2MASS sources that is detected by *IRAS* and we calculated the FIR luminosity of J0441 from the *IRAS* fluxes according to Sander & Mirabel (1996, their Tab. 1). This yields $L_{\text{FIR}} \sim 5 \cdot 10^{12} L_{\odot}$. Thus, J0441 easily qualifies as a type–2 AGN/ULIRG. We detect PAHs only of small equivalent width. The MIR spectrum resembles that of the FIR luminous dust rich broad–line quasar PG0157+001 (Mrk 1014 Armus et al. 2004) and possibly is an intermediate case between Mrk 273 and PG0157+001.

6.2.2 J1232

In the optical, J1232 displays a red continuum. There are only very few clear absorption lines present with Ca II K being the most prominent (Fig. 6.2). No clear absorption signature can be identified in the spectrum of J1232, neither a Balmer jump nor a 4000 Å break. This indicates that most stellar features may have been diluted by a

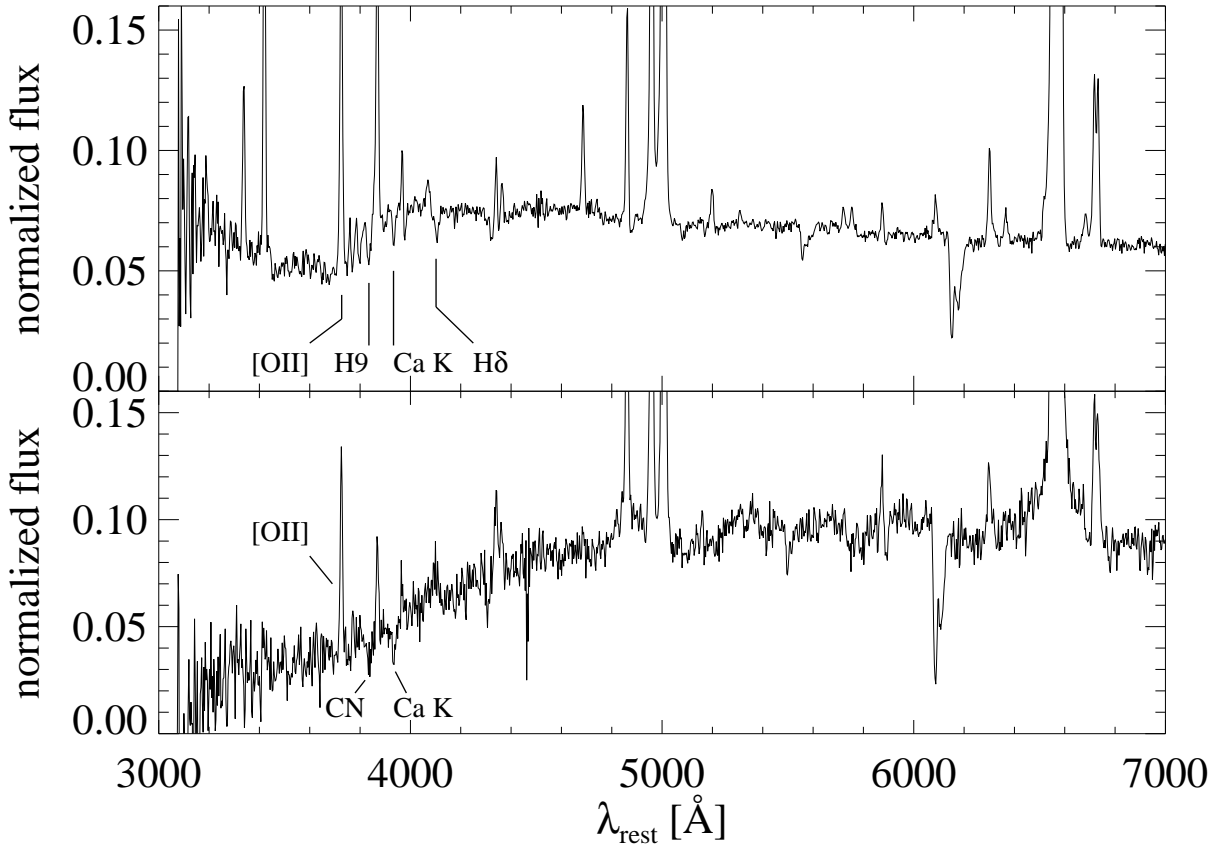


Figure 6.2: Enlarged view of the optical continuum of J0441 (*top*) and J1232 (*bottom*) to illustrate the difference in the host galaxies.

non-stellar continuum. Since Ca II K is visible and higher order Balmer absorption lines are not, it is unlikely that the young stellar population is strong in this object. This is supported by the low FIR emission, i.e. the flat spectrum towards FIR wavelengths (Fig. 6.1, *lower right*).

Focussing on the emission-lines in the spectrum of J1232 we see that [Ne V] is not detected whereas it was even stronger than [O II] in J0441. This can be caused by obscuration of the regions where [Ne V] is emitted, i.e. the inner regions of the NLR with the necessary high-energy photons. In this case the obscuring dust has to be located mainly in the inner parts of the NLR.

Remarkably, we also see broad emission-line components at the bases of H α and H β (Fig. 6.2), indicating that J1232 has rather to be classified as a type-1.8 according to Osterbrock (1977). This also indicates that the central region of the AGN is possibly viewed under an intermediate angle by grazing the torus edge and allowing some emission from the BLR to be visible. Alternatively, light from the broad-line region could be scattered into the line of sight.

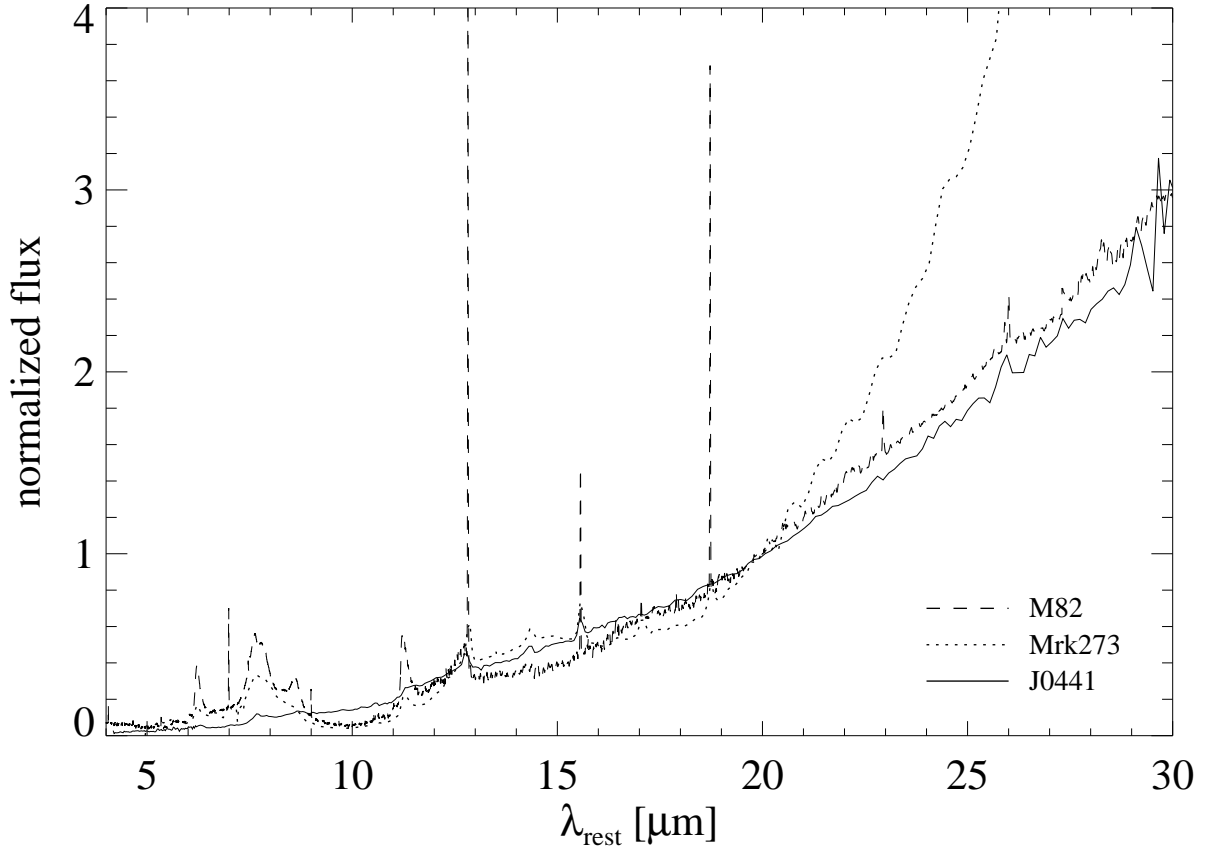


Figure 6.3: Comparison of the MIR spectra of J0441, M82, and Mrk273. The spectra are normalised to their flux at $20 \mu\text{m}$. The ISO–SWS spectrum of M82 was taken from Sloan et al. (2003).

However, in any case, this means that we also expect the featureless continuum (FC) from the active nucleus to be present in the spectrum (e.g. Cid Fernandes et al. 2004). In this case, the scattered FC dilutes the absorption lines, especially in the blue where the FC is stronger and the scattering efficiency is larger. But the optical continuum of J1232 is red despite the contribution of an intrinsically blue FC suggesting considerable dust reddening. This is confirmed by an emission–line ratio of $\frac{H\alpha}{H\beta} \sim 6$ corresponding to $A_{V,NLR} \sim 2$ (narrow component).

We estimate A_V also from the silicate absorption (Fig.6.1, lower right) and get $A_{V,MIR} \approx 6 - 7$ (following Krügel 2003)¹. Since $A_{V,NLR}$ is only an average value for the NLR, the difference in the A_V values indicates that the absorption for the NLR gas and the MIR continuum takes place at different regions in the galaxy. Since most of the NLR emission comes from scales large compared to the MIR continuum source,

¹ We estimated the flux of the pseudo–continuum at the position of the silicate feature (I_0) as well as the observed flux (I). While $I = I_0 \cdot e^{-\tau}$ and $A_\lambda = 1.086 \tau_\lambda$, we calculated $A_{V,MIR}$ using $A_V \approx 17 \cdot A_{9.7\mu\text{m}}$ with $\tau_{9.7\mu\text{m}} \approx 0.32 - 0.38$.

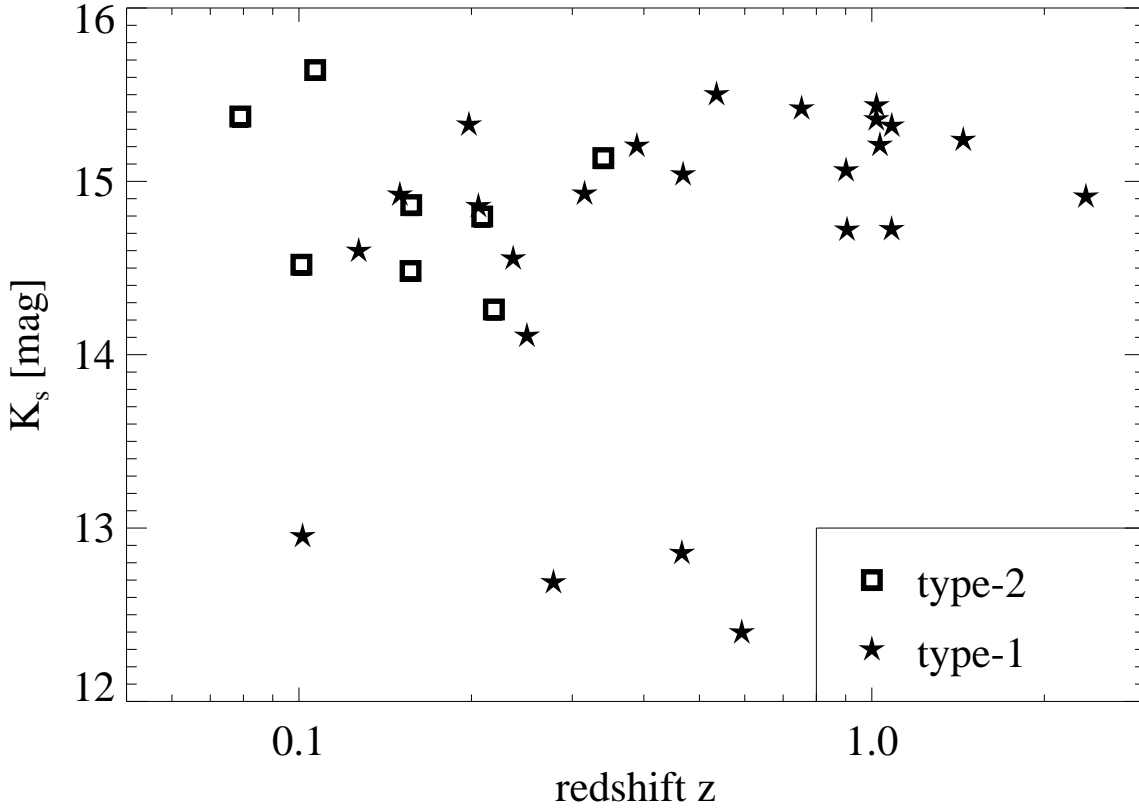


Figure 6.4: K_s versus z distribution for the ISO-2MASS AGN.

we suggest that the silicate absorption is mainly due to obscuration in the inner parts of the galaxy. Additionally the NLR emission and the MIR continuum is absorbed by ambient dust in the host galaxy. This dust distribution fits well with our findings that the emission of highly ionised gas in the inner parts of the NLR is possibly obscured by dust.

If the dust is concentrated towards the central regions of the NLR we may assume that this dust can serve as the scattering medium for radiation from the central regions hidden in direct light (e.g. broad Balmer lines). If the inner parts of the AGN harbour large amounts of dust, the AGN continuum may suffer reddening already before being scattered to dilute the stellar absorption lines.

This may explain in parts the red (featureless) continuum observed in the optical. Moreover, the red optical continuum shape despite a significant amount of AGN continuum is not unlikely since there are also type-1 AGN known that show red optical continua (e.g. Smith et al. 2003; Leipski et al. 2005).

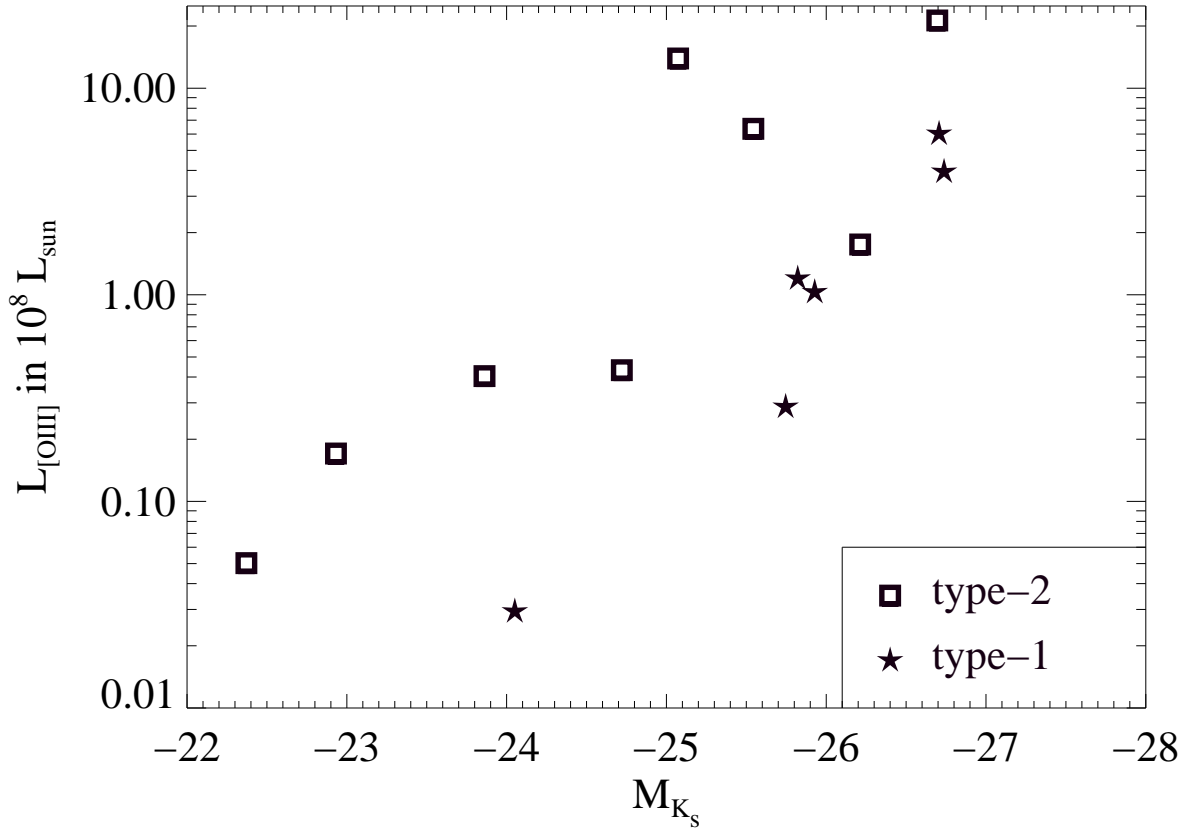


Figure 6.5: Luminosity in the [O III] emission line plotted versus the absolute K_s magnitude.

6.2.3 Comparison of type-1 and type-2 objects

For surveys relying on isotropic properties (e.g. using 178 MHz fluxes Laing et al. (1983); Spinrad et al. (1985) or FIR data Keel et al. (2005)) the ratio of type-1 to type-2 AGN turns out to be ~ 1 . Surveys in the MIR using the four Spitzer IRAC filters find also a ratio of ~ 1 (e.g. Lacy et al. 2004a,b).

In total, our NIR-MIR approach finds three times more type-1 sources than type-2 sources. However, the inspection of Fig. 6.4 shows that at higher redshifts ($z \geq 0.4$) no narrow-line AGN has been found. In fact, the numbers of type-1 and type-2 AGN are approximately the same at lower redshifts, in agreement with the findings from other surveys.

To understand this behaviour, we first consider the origin of the different parts of the SED of type-2 objects. The hot dust that is seen as continuum emission in the NIR most likely originates at the inner surface of the obscuring torus that is heated by the central engine. At higher z only the hottest dust ($T > 1000$ K) is observable in the NIR filters.

In type-2 objects the torus is thought to be inclined in such a way that the inner regions are hidden to the observer. Therefore, the extinction of the most central and hottest dust emission by the torus or the torus edge leads to a loss in magnitude and the source shifts below our magnitude cutoff ($K_s < 15.5$ mag). Additionally, the NIR colours (e.g. $H - K_s$) become bluer because host galaxy contributions become important when the hottest AGN related dust components are absorbed. However, at $H - K_s < 0.5$ we only find $\sim 5\%$ type-2 objects². Therefore we conclude that the magnitude limit is the main reason for the lack of high- z type-2 AGN in the ISO-2MASS sample.

If the hottest dust emission is affected by extinction in type-2s, then such AGN have to be intrinsically more luminous than type-1s to be selected by our survey. We can test this picture by assuming that the luminosity of the [O III] emission-line is a good measure for the total luminosity of the central engine (e.g. Zakamska et al. 2003). This was possible for the eight type-2s and for six type-1s with $z < 0.5$ and $K_s > 14$ mag.

The distributions of the [O III] luminosities shows no difference between type-1 and type-2 AGN (Fig. 6.5). However, from Fig. 6.5 it is obvious that the absolute K_s magnitude at a given $L_{[\text{O III}]}$ is fainter for type-2 sources than for type-1s. This supports the idea that type-2 AGN are extinct also in the NIR.

The selection of type-2 AGN via the ISO-2MASS colours is successful up to $z \sim 0.5$ and the ratio of type-1 and type-2 sources is ~ 1 in this range. The NMIR selection finds more type-1 objects than, for example, the SDSS survey (Leipski et al. 2005). It is worth mentioning that due to this increase in type-1 surface density the number of type-2 AGN correspondingly increases.

6.3 Conclusions

We find eight type-2 AGN at redshift $0.1 < z < 0.4$, three of them have even quasar-like [O III] luminosities. At the given redshift and luminosity range the number of type-2 AGN equals that of type-1s.

The type-2 sources show a high diversity of spectral properties, including their stellar populations and the amount of existing dust.

The mid-infrared 5–30 μm spectra of the two type-2 sources show – superimposed on a power-law continuum – PAH emission and silicate absorption which we suggest to originate in the host galaxy.

The near-mid-infrared selection of type-2 AGN is a successful strategy, but this class of objects turns out to exhibit a diversity of observed properties at least as high as the type-1 AGN.

² At $H - K_s < 0.5$ we have 56 objects of which 24 randomly selected have optical spectroscopy available. Only one source turns out to be a type-2 AGN.

Summary and outlook

7.1 Summary

A promising new strategy to search for AGN independent of dust extinction was presented. The ISO-2MASS AGN survey revealed AGN candidates by their characteristic near-to-mid infrared colours, taking advantage of the *ISOCAM Parallel Mode Survey* at $6.7\mu\text{m}$ in combination with the *Two Micron All Sky Survey*. By means of optical follow-up spectroscopy the redshift and the classification of the candidates were determined. Type-1 and type-2 AGN as well as unusually red emission-line galaxies have been found.

Focusing on the AGN in the survey it was demonstrated that the surface density of the ISO-2MASS quasars exceeds that of the SDSS by 50%. This increase is due to a population of reddened type-1 AGN that are included in the infrared survey but excluded by optical techniques.

The reddest type-1 source in the survey has been further explored in the optical and in the infrared, revealing an interacting companion near the quasar. The quasar shows no sign for a strong young stellar population, unlike its companion which had a burst of star formation a few hundred millions years ago. The spectrum of the quasar also revealed that the optical AGN continuum is heavily reddened while the broad emission lines are still unabsorbed. This requires a spatial distribution of obscuring material where a dense absorber needs to cover the continuum source but not the BLR.

Studying the narrow-line AGN found by the ISO-2MASS survey the diversity of type-2 spectra at optical as well as at MIR wavelengths was emphasised. One object, for example, displays strong MIR and FIR emission that qualifies it as a type-2 AGN/ULIRG. The FIR emission is supposed to originate from star formation and in fact the optical spectrum shows the blue continuum and the absorption lines indicating young and intermediate-age stars.

Another narrow-line object displays a dust reddened continuum in the optical and considerable silicate absorption in the MIR. However, broad wings in the line profiles of $\text{H}\alpha$ and $\text{H}\beta$ were detected, indicating either a view at intermediate angles or the

scattering of light from the BLR. I favour the latter suggestion since the dust responsible for the reddening of the continuum and the emission lines can also serve as the scattering medium for the broad line wings.

The comparison between the type-1 and the type-2 sources showed that the ISO-2MASS survey finds type-2 AGN only at $z < 0.5$. It seems that type-2 AGN are more extinct at NIR wavelengths, therefore such sources have to be intrinsically more luminous than type-1 AGN to reach the NIR magnitude cut-off.

It turns out that the ISO-2MASS AGN survey is a valuable tool for finding obscured as well as unobscured AGN via their infrared properties.

7.2 Outlook

During selection numerous objects have been excluded for different reasons and they could be investigated to enlarge the sample. However, to avoid contamination by stars or by ambiguous NIR and optical counterparts it is necessary to inspect the individual sources carefully.

Furthermore, prior to the candidate selection process ~ 100 sources with *ISO* photometry but without 2MASS counterpart have been found. NIR photometry of these sources was obtained and a large number of them fulfil the colour criteria ($H - K_s > 0.5$ and $K_s - LW2 > 2.7$). The optical spectroscopy revealed that many of these “ISOCAM-only” sources are AGN, with a high fraction of $z \sim 1$ quasars. These objects are currently being explored but complete photometric ($\sim 70\%$) and spectroscopic ($\sim 70\%$) coverage is not yet achieved.

In addition to the AGN presented in this thesis, a population of 45 emission-line galaxies with very red NIR colours has been found among the 77 ISO-2MASS AGN candidates. While these sources exhibit a wide range of spectral properties in the optical, their MIR spectra are generally cool and show prominent PAH emission. They are suggested to represent a population of cool and dusty galaxies with enhanced star formation. These emission-line galaxies are also currently being explored.

Bibliography

- Abazajian K., et al. 2003, AJ 126, 2081
- Adelman–McCarthy, J. K., Agüeros, M. A., Allam, S. S., et al. 2006, ApJS, 162, 38
- Antonucci, R. R. J. & Miller, J. S. 1985, ApJ, 297, 621
- Antonucci, R. R. J. 1993, ARA&A, 31, 473
- Armus, L., Charmandaris, V., Spoon, H., et al. 2004, ApJS, 154, 178
- Barkhouse W.A. & Hall P.B., 2001, AJ 121, 2843
- Bennett, C. L., Halpern, M., Hinshaw, G. et al. 2003, ApJS, 148, 1
- Boselli A., Lequeux J., Sauvage M., et al., 1998, A&A 335, 53
- Buchanan, C. L., Gallimore, J. F., O’Dea, C. P., Baum, S. A., Axon, D. J., Robinson, A., Elitzur, M., Elvis, M. 2006, to appear in “Infrared Diagnostics of Galaxy Evolution”, astro-ph/0603442
- Cesarsky, C. J., Abergel, A., Agnese, P., et al. 1996, A&A, 315, L32
- Cid Fernandes, R., Gu, Q., Melnick, J., Terlevich, R., et al. 2004, MNRAS, 355, 273
- Clavel J., Schulz B., Altieri B., et al., 2001, A&A 357, 839
- Croom, S. , Smith, R. , Boyle, B. , et al. 2004, MNRAS, 349, 1397
- Cutri R.M., Nelson B., Kirkpatrick J., et al., 2001, AAS 198, 3317
- Cutri, R. , Nelson, B. , Francis, P., Smith, P. 2002, ASP 284, 127
- Cutri R.M., Skrutskie M.F., van Dyk S., et al., 2003, ”2MASS All-Sky Catalog of Point Sources”, VizieR On-line Data Catalog: II/246 Kolhatkar S., 2001, ApJ 549, 215
- Dale D.A., Helou G., Contursi A., et al., 2001, ApJ 549, 215 2001, ASP Conf. Ser. 225, 52

- Djorgovski S., Mahabal A., Brunner R. et al., 2001, ASP Con. 225, 52
- Francis P.J., Nelson B.O., Cutri R.M., 2004, AJ 127, 646
- Glikman, E., Gregg, M. D., Lacy, M., et al. 2004, ApJ, 607, 60
- Haas M., Klaas U., Müller S.A.H., et al., 2001, A&A 367, L9
- Haas M., Klaas U., Müller S.A.H., et al., 2003, A&A 402, 87
- Haas, M., Siebenmorgen, R., Leipski, C., et al. 2004, A&A, 419, L49
- Haas M., Müller S.A.H., Bertoldi F., et al., 2004, A&A, 424, 531
- Haas, M., Siebenmorgen, R., Schulz, B. 2005, A&A, 442, L39
- Ho, L. C. 2005, ApJ, 629, 680
- Houck, J. R., Roellig, T. L., van Cleve, J., Forrest, W. J., Herter, T., Lawrence, C. R., Matthews, K., Reitsema, H. J., et al. 2004, ApJS, 154, 18
- Keel, W. C., Irby, B. K., May, A., Miley, G. K., Golombek, D., de Grijp, M. H. K., Gallimore, J. F. 2005, ApJS, 158, 139
- Kewley, L. J., Dopita, M. A., Sutherland, R. S., Heisler, C. A., & Trevena, J. 2001, ApJ, 556, 121
- Klaas U., Haas M., Müller S.A.H., et al., 2001, A&A 379, 823
- Krügel, E. 2003. The Physics of Interstellar Dust (Bristol: Institute of Physics Publishing)
- Lacy, M., Storrie-Lombardi, L., Sajina, A., et al. 2004, ApJS, 154, 166
- Lacy et al. 2004, astro-ph/0411416
- Lacy, M., Canalizo, G., Rawlings, S., Sajina, A., Storrie-Lombardi, L., Armus, L., Marleau, F. R., and Muzzin, A. 2005, MmSAI, 76, 154
- Laing, R. A., Riley, J. M., Longair, M. S. 1983, MNRAS, 204, 151
- Laurent O., Mirabel I.F., Charmandaris V., et al., 2000, A&A 359, 887
- Leipski, C., Haas, M., Meusinger, H., et al. 2005, A&A, 440, L8
- Liebert J., Cutri R.M., Nelson B., et al., 2000, PASP 112, 1315
- Low, F., Cutri, R., Huchra, J., & Kleinmann, S. 1988, ApJ, 327, L41
- Maiolino, R., Comastri, A., Gilli, R., et al. 2003, MNRAS 344, L59

- Mann R.G., Oliver S., Carballo R., et al., 2002, MNRAS 332, 549
- Marble, A. R., Hines, D. C., Schmidt, G. D., Smith, P. S., Surace, J. A., Armus, L., Cutri, R. M., Nelson, B. O. 2003, ApJ, 590, 707
- Meisenheimer, K., Haas, M., Müller, S. A. H., Chini, R., Klaas, U., and Lemke, D. 2001, A&A, 372, 719
- Miller, J. S., Goodrich, R. W., & Mathews, W. G. 1991, ApJ, 378, 47
- Monet, D. G., Levine, S. E., Canzian, B., et al. 2003, AJ, 125, 984
- Norman, C., Hasinger, G., Giacconi, R., Gilli, R., et al. 2002, ApJ, 571, 218
- Ogle, P. M., Whyson, D., & Antonucci, R. 2006, astro-ph/0601485
- Oliver S., Mann R. G., Carballo R., et al., 2002, MNRAS 332, 536
- Osterbrock D. E. 1977, ApJ, 215, 733
- Ott S., Siebenmorgen R., Schartel N., Vö T., 2003, ESA SP-511, 159
- Ott, S., Siebenmorgen, R., Schartel, N., et al. 2006, A&A, submitted
- Ptak A., Heckman T., Levenson N. A., et al. 2003, ApJ592, 782
- Richards, G. T., Fan, X., Newberg, H. J., et al. 2002, AJ, 123, 2945
- Richards, G. T., Hall, P. B., Vanden Berk, D. E., Strauss, M. A., Schneider, D. P., et al. 2003, 126, 1131
- Rowan–Robinson M., Lari C., et al. 2003, MNRAS, 351, 1290
- Sandage A. & Wyndham J. D., 1965, ApJ 141, 328
- Sanders, D., Soifer, T., Elias, J., et al. 1988, ApJ325, 74
- Sanders, D. B. & Mirabel, I. F. 1996, ARA&A, 34, 749
- Satyapal S., Sambruna R., Dudik R. P., 2004, A&A 414, 825
- Schmidt, M. & Green, R. F. 1983, ApJ, 269, 352
- Schneider, D., Hall, P., Richards, G., et al. 2005, AJ, 130, 367
- Sloan, G. C., Kraemer, K. E., Price, S. D., and Shipman, R. F. 2003, ApJS, 147, 379
- Smith J. A., Tucker D., Kent S., et al. 2002, AJ 123, 2121
- Smith, P. S., Schmidt, G. D., Hines, D. C., & Foltz, C. B. 2003, ApJ, 593, 676

- Siebenmorgen R., Abergel A., Altieri B., et al., 1996, *A&A* 315, L169
- Siebenmorgen R., Freudling W., Krügel E. et al. 2004, *A&A* accepted
- Spinrad H., et al. 1985, *PASP*, 97, 932
- Urry C. M. & Padovani P., 1995, *PASP* 107, 803
- Väisänen P., Morel, Rowan-Robinson, et al., 2002, *MNRAS* 337, 1043
- Vanden Berk, D. E., Richards, G. T., Bauer, A., Strauss, M. A., Schneider, D. P., et al. 2001, *AJ*, 122, 549
- Vanden Berk, D., Schneider D., Richards G., et al. 2005, *AJ*, 129, 2047
- Veilleux, S. & Osterbrock, D. E. 1987, *ApJS*, 63, 295
- Véron-Cetty M. P. & Véron P., 2003, *A&A* 412, 399
- Vignali, C., Alexander, D. M., & Comastri, A. 2004, *MNRAS*, 354, 720
- Webster R., Francis P., Peterson B., et al., 1995, *Nature* 375, L469
- Weedman, D. W., Hao, L., Higdon, S. J. U., Devost, D., Wu, Y., Charmandaris, V., Brandl, B., Bass, E., Houck, J. R. 2005, *ApJ*, 633, 706
- Werner, M. W., Roellig, T. L., Low, F. J., Rieke, G. H., Rieke, M., Hoffmann, W. F., Young, E., Houck, J. R., et al. 2004, *ApJS*, 154, 1
- Wilkes B. J., Schmidt G. D., Cutri R. M., et al., 2002, *ApJ* 564, L65
- Wilkes, B. J., Risaliti, G., Ghosh, H et al. 2003, *BAAS* 203, 6304
- Wilkes, B. J., Pounds, K. A., Schmist, G. D., Smith, P. S., Cutri, R. M., Ghosh, H., Nelson, B., and Hines, D. C. 2005, *ApJ*, 634, 183
- Wisotzki, L., Christlieb, N., Bade, N., et al. 2000, *A&A*, 358, 77
- Wolf, C., 2005, *MmSAI* 76, 21
- York, D. G., Adelman, J., Anderson, J. E. Jr., et al. 2000, *AJ*, 120, 1579
- Zakamska N. L., Strauss M. A., Krolik J. H., et al., 2003, *AJ* 126, 2125
- Zakamska, N. L., Schmidt, G. D., Smith, P. S., Strauss, M. A., Krolik, J. H., Hall, P. B., Richards, G. T., Schneider, D. P., Brinkmann, J., Szokoly, G. P. 2005, *AJ*, 129, 1212

Curriculum Vitae

Personal data

Name: Christian Leipski
Date of birth: December 30th 1977
Place of birth: Essen, NRW, Germany
Nationality: German

Education

June 1997
Abitur (Highschool Diploma; Gymnasium Essen–Überruhr, Essen, Germany)

Oct 1998 – Sep 2000
Undergraduate student of physics, mathematics, and astronomy
at the Ruhr–University Bochum (RUB)

Oct 2000
Pre-degree (Vordiplom; B.Sc.) in physics (RUB)

Oct 2000 – Nov 2002
Graduate student of physics/astrophysics

Dec 2002 – Dec 2003
Diplom student (Master’s student) working on Active Galactic Nuclei

Dec 2003
Diplom (Master’s degree) in physics (RUB)
Title of thesis: “Radioemission von Aktiven Galaktischen Kernen”
(Radio emission of active galactic nuclei)
Advisor: PD Dr. S. Hüttemeister

Jan 2004 – present
PhD student (Astronomical Institute of the Ruhr–University Bochum)
Title of thesis: “The ISO–2MASS AGN Survey”
Advisors: Prof. Dr. R. Chini, Dr. habil. M. Haas